Abstract

PISONI, JOSEPH JUSTIN. Experimental Estimation of Power Effects on Neutral Point Location. (Under the direction of Charles E. Hall, Jr.)

Two approaches were taken to estimate the power effects on the neutral point of an unmanned aerial vehicle (UAV). The first approach was the solution of two simultaneous equations for the aircraft pitch stiffness, $C_{m\alpha}$. The second approach was the comparison of a computer code predicted, power-off neutral point location to a flight data estimated power-on neutral point. The approaches are explained and each was attempted.

Flight-testing was conducted with a UAV weighing 23 lbs. and a wingspan of 7.5 ft. The solution of two simultaneous equations was not completed due to flight-testing mishaps and time constraints. This failure led to the second approach. The computer code/flight estimation of power effects on the neutral point was completed. The power effects were used to estimate the change in the propeller normal force with changes in angle of attack, $(C_{Np})_{\alpha}$, for the UAV. $(C_{Np})_{\alpha}$ was compared to historical estimates to determine if reasonable results for the power effects were obtained. Aircraft designers can use these estimates to better predict static stability of future aircraft designs.

EXPERIMENTAL ESTIMATION OF POWER EFFECTS ON NEUTRAL POINT LOCATION

by

JOSEPH JUSTIN PISONI

A thesis submitted to the Graduate Faculty of
North Carolina State University
in partial fulfillment of the
requirements for the Degree of
Master of Science

AEROSPACE ENGINEERING

Raleigh

2003

APPROVED BY:

_____
Amassa Fauntleroy, Ph.D. Advisory Committee Member
Dept. of Mathematics

_____
Ashok Gopalarathnam, Ph.D., Advisory Committee Member
Dept. of Mechanical and Aerospace Engineering

_____
Charles E. Hall, Jr., Ph.D., Advisory Committee Chair
Dept. of Mechanical and Aerospace Engineering

Dedication

This is dedicated, first and foremost to my wife, Ruie, and son, Joey. Without their constant support, encouragement, and sacrifice, this would not have been possible. I can't say or do enough to thank you for being there for me and pushing me. You teach me something new everyday.

This is dedicated to my parents, Joe and Judy, without their love, guidance, and support, I would not be who or where I am today, and to my in-laws, John, Mary, and Bonnie, who inspire me with their experiences and encouragement.

Biography

Joseph Justin Pisoni was born to Joseph Mark Pisoni and Judith Ann Pisoni in Dubois, PA. He has one younger brother and three younger sisters. He graduated from Brocton Central High School in western New York in 1995 and attended Salem-Teikyo University in Salem, West Virginia, where he met his wife, Ruie. Searching for a more interesting and well-funded existence, Joe left Salem and enlisted in the United States Navy in 1997.

In 1999 Joe qualified as a Navy Nuclear Reactor Operator/Electronics Technician and was ordered to North Carolina State University to earn a Bachelor's Degree. In June 2001 Joe and Ruie's first child, John Joseph Pisoni, was born, and in 2002, Joe graduated Magna Cum Laude with a Bachelor of Science Degree in Aerospace Engineering.

Joe is currently working on a Master of Science Degree in Aerospace Engineering at North Carolina State University. He is an Ensign in the United States Navy and is headed to Charleston, SC for training as a Naval Submarine Nuclear Propulsion Officer.

Acknowledgements

I would like to express my deepest gratitude to all those who helped me through my career at North Carolina State University. I would like to thank the advisory committee, Dr. Charles Hall, Dr. Ashok Golpalarathnam, and Dr. Fauntleroy, for the guidance and knowledge they shared with me. I would especially like to thank Dr. Hall for his patience, time, and for piloting the UAVs.

I would like to thank Stearns Heinzen, Sean Angermuller, Will Barnwell, Rob Burgun, and Wallis Collie. Thanks for putting up with me and questions I asked. Your ideas and generosity were vital to this project's completion.

I would also like to thank the Unites States Navy for its financial support and granting me this opportunity. Particularly, LCDR Mark Cooper, for his guidance and assistance in making this opportunity a reality, and LT Jason Geddes for his guidance and for looking out for me when I needed it most.

Finally, I would like to thank my family, Ruie, Joey, Mom, Dad, Julian, Jessica, Jennifer, Justine, John, Mary, Bonnie, Audrey, Justin, Dylan, and Jackson. Your support and encouragement keep me going. To Dylan, may the force be with you young Jedi. Jackson, "What did you call me?" Both of you, don't ever give up! Anything is possible!

Table of Contents

List of Tables

List of Figures

CHAPTER 2

CHAPTER 3

CHAPTER 4

List of Symbols

AR	aspect ratio, b^2/S
a_o	two-dimensional lift slope, $\partial C_l / \partial \alpha$
b	wingspan
C_L	lift coefficient, L/ (q S)
$C_{L\ trim}$	trim lift coefficient
$C_{L\alpha}$	airplane lift slope curve,
$C_{L\delta e}$	$\partial C_L / \partial \delta e$
$(C_{L\delta e})_t$	$\partial C_L / \partial \delta e$ referenced to the tail area
C_l	two-dimensional lift coefficient
C_m	airplane pitching moment coefficient
C_{mo}	airplane pitching moment coefficient at zero α
$(C_{mo})_w$	wing contribution to C_{mo}
$(C_{mo})_f$	fuselage contribution to C_{mo}
$C_{m\alpha}$	pitch stiffness, $\partial C_m / \partial \alpha$
$(C_{m\alpha})_p$	power-on $\partial C_m / \partial \alpha$
$(C_{m\alpha})_{prop}$	propulsion contribution of $\partial C_m / \partial \alpha$
$C_{m\delta e}$	$\partial C_m / \partial \delta e$
$(C_{Np})_\alpha$	change in propeller normal force coefficient with α
$\bar{c}$	mean aerodynamic chord
h	center of gravity, $x_{cg} / \bar{c}$
h_n	neutral point, $x_n / \bar{c}$
$(h_n)_p$	power-on neutral point, $(x_n)_p / \bar{c}$
h_{wb}	wing/body aerodynamic center
i_w	wing incidence angle
i_t	tail incidence angle
K	propeller wash coefficient
L	lift

l_p	distance from cg to propeller
l_t	distance from cg to tail aerodynamic center
$\bar{l}_t$	distance from h_n to tail aerodynamic center
M	pitching moment
N_p	propeller normal force
q	dynamic pressure, $\frac{1}{2} \rho V^2$
q_t	tail dynamic pressure
q_w	wing dynamic pressure
S	wing area
S_p	propeller area
V	velocity
V_H	tail volume ratio, $\bar{l}_t S_t / \bar{c} S$
W	weight
x_{cg}	center of gravity x location measured from the nose
x_n	neutral point x location measured from the nose
$(x_n)_p$	power-on neutral point x location measured from the nose
$x_{n\ wb}$	wing body aerodynamic center x location measured from the nose
α	angle of attack referenced to aircraft zero lift angle of attack
α_{eff}	effective angle of attack
α_{trim}	trim angle of attack referenced to aircraft zero lift angle of attack
α_p	propeller angle of attack
$\Delta C_{mo\ flex}$	change in C_{mo} due to flexing
δe	elevator deflection
δe_{trim}	trim elevator deflection
$\delta e_{C_{L\ trim\ zero}}$	elevator deflection at $C_{L\ trim} = 0$
ε_p	upwash at the propeller
ε_t	downwash at the tail
ε_o	downwash at tail at zero angle of attack
η	propeller efficiency factor, q_t/q_w
ρ	air density

List of Abbreviations

cg	center of gravity
FCS	flight computer system
g	gravitational acceleration
NCSU	North Carolina State University
NP	neutral point
UAV	unmanned aerial vehicle

1 INTRODUCTION

1.1 BRIEF UNMANNED AERIAL VEHICLE HISTORY

Crude unmanned aerial vehicles (UAVs) have been used as far back as the Civil War[1, 2]. In 1863, Charles Perley patented an unmanned aerial bomber[2]. He placed explosives in a basket under a hot air balloon and used a timer to release the explosives, hoping the cargo would land in an enemy ammunition store. As one might imagine, the lack of control over the "UAV" and air currents made this very ineffective and the practice did not last long.

In 1917, Elmer Sperry and Dr. Peter Cooper invented the *Sperry Aerial Torpedo*. It was a converted US Navy Curtiss N-9 trainer, designed to automatically fly a preset distance and then dive onto its target with an explosive payload[3]. In the same year, the US Army gave Charles Kettering the money to build 50 *Kettering Aerial Torpedoes*, nicknamed the "Bug"[4]. The Bug was a wood laminate and papier-mâché UAV designed to carry a 300-lb bomb. It was dolly launched down a track aimed in the target's direction. A timer circuit on the aircraft would shut down the engine, cause the wings to fall off, and the fuselage and warhead would fall to the target. Initial tests for both aerial torpedoes were successful, but the war ended before they were used in combat and the funding was cut.

The development and use of UAVs continued to grow. In the 1920's, one of the world's leading aircraft reference books, *Jane's All the World's Aircraft*, began listing UAVs[5]. In the 1930's, the Royal Navy began using the *Queen Bee*, the first re-usable and

returnable UAV, for target practice for anti-aircraft gunnery training[2]. In World War II, UAVs were still used as target drones, but they were no longer just targets.

Germany developed the V-1. It carried a 2000-lb warhead and is credited with killing or injuring over 35,000 British civilians in 1944. To counter the V-1, the US converted Liberator's and B-17's into what may be loosely called UAVs. The converted aircraft, designated PB4Y-1 and BQ-7, were flown by onboard pilots during take-off. After take-off, the pilots set the aircraft's course and bailed out. The typical target for the 25,000-lb explosive payload was the launch site of the V-1's. This marked the first time one UAV was used against another. [2]

The role of the UAV continued to expand. By 1964 the United States had its first photoreconnaissance UAV, BQM-34 Ryan Aeronautical *Lightning Bug*. From a simple photoreconnaissance UAV, the *Lightning Bug* evolved and was used in the Vietnam War to provide battle damage assessments, gather electronic intelligence, drop leaflets, and provide real-time video. During the Persian Gulf War, the *Pioneer* UAV system, used in combination with other military platforms, provided gunfire support, target acquisition, reconnaissance, and battle damage assessment as never seen before. [4]

Predator, an American UAV most recently used in the war on terror, represents one of the most technologically advanced UAVs on the planet. *Predator* was designed to provide reconnaissance, surveillance, and target acquisition. However, it has been outfitted with Hellfire missiles, making it capable of firing on an enemy target and returning home. [6]

Today unmanned aerial vehicle development and their uses continue to grow. UAVs are being used more often, in more roles, and in more countries, for three major

reasons. First, technological advances, such as electronics, battery life, and composite materials, have increased UAV capabilities. Second, UAVs reduce the potential for loss of human life. Finally, UAVs are a fraction of the cost of their manned counterparts. The United States Navy's newest operational multi-mission tactical aircraft, the F/A-18E *Super Hornet*, is $57 million dollars per aircraft, excluding pilot training[7]. *Predator* is less than $4 million per aircraft and does not risk the life a highly trained pilot[8].

Today, both civilian and military organizations from around the world use UAVs. *Aerosonde*, *ALO*, and *Firebird 2001*are three examples. *Aerosonde*, is manufactured in Australia and used in environmental and meteorological surveys, radio relay, military and coastal surveys, and mining and agricultural surveys[9]. *ALO*, is manufactured in Spain, and used for target acquisition, fire detection & monitoring, and reconnaissance[9]. *Firebird 2001*, an Israeli UAV, is used to deliver real-time, information on a wildfire's size, speed, perimeter, and movement[2].

UAVs have become so common, cost effective, and useful that university students are required to manufacture them as part of their undergraduate coursework. North Carolina State University has required its aerospace engineering senior design class to design and build UAVs since 1977. NCSU's UAVs have been used for a wide range of research topics, including this one.

1.2 MOTIVATION

One of the obstacles encountered by aircraft designers is the prediction of power effects on the static stability. Research is readily available from World War II studies of the power effects, but is limited to the aircraft characteristics of the time[10-13]. Currently,

the wide range of propulsion units and variations in aircraft geometry has hindered the development of a comprehensive approach to predicting the effects of power on static stability[13]. To determine the power effects, expensive wind tunnel testing is often required[14,15].

Estimating the power effect on the neutral point from flight-test data will provide future designers of similar UAVs with a reference to make their own estimates and better predict the static stability of their design. The future expansion of this research to many other UAVs with different power configurations may generate enough experimental data to compile the power effects on the neutral point into a single reference source, basing the power effects on UAV geometry and power configuration. Future designers could use this reference source to make their own estimates of the power effects by comparing the geometry and power configuration of their design to those already estimated in the reference source. If enough experimental data is recorded, comprehensive predictive theory may also be developed from the data. This would reduce the need for wind tunnel testing and lower the risk of redesign due to poor power effect estimates.

1.3 OBJECTIVES

The objective of this work is to estimate the effect power has on the neutral point of a UAV. A by-product of the approach taken here, is an estimate of $(C_{Np})_{\alpha}$, another contributor to the static stability of an aircraft. Values for both estimates will be useful tools for designers of UAVs similar to the test vehicle.

1.4 OVERVIEW

An approach is developed to estimate the power effects on the neutral point of a UAV. The theory explained shows how two simultaneous equations and flight data could be used to make the estimate. The two equations relate the power-off neutral point to the power-on neutral point, and require flight testing data from a single aircraft whose geometry would not change when the engine/propeller configuration was switched from tractor to pusher or vice versa. The propellers for each configuration were identical, with the obvious exception of one being for tractor and one being for pusher.

Two vehicles were used for flight-testing and both suffered damage, eliminating them from use. The first test vehicle was lost on its first flight due to improper cargo loading. No flight data was collected. The second UAV presented a new problem. The tail of the aircraft was attached to the fuselage by two booms. The booms were not as longitudinally rigid as desired, and introduced an aeroelastic effect. The effect was assumed to be minimal and flight-testing was continued.

Sufficient flight data was obtained for the tractor-configuration, but the UAV was severely damaged on its first attempt to collect pusher-configuration data. The damage was beyond repair with-in the time constraints of the project and a new approach to estimate the power effects was employed.

The power-off neutral point was estimated using an established computer code. The code analyzes three-dimensional closed surface models, assuming irrotational, incompressible flow, and obtains the solution for the potential flow. From this aerodynamic properties of the model are obtained.

The power-on neutral point was estimated from flight data. The flight data was processed two ways. The first processing method yielded unrealistic results. This lead to the discovery that not all flight data was useful. Reasonable estimates for the power effects on the neutral point and $(C_{Np})_{\alpha}$ were obtained by processing the useful flight data.

2 APPROACH

2.1 INTRODUCTION

Determining the relationship between changes in angle of attack, α, and pitching moment about the center of gravity, cg, is simplified by use of the neutral point of an aircraft. The neutral point, also known as aircraft aerodynamic center, is the location on an aircraft about which the pitching moment remains constant with changing α. The neutral point plays a vital role in static stability.

Static stability is a function of the static margin and requires a negative slope of C_m versus α (defined as positive pitch stiffness) (Figure 2.1). The static margin is the distance from the cg to the neutral point, $h - h_n$, where h is the cg position and h_n the neutral point, both measured from a fixed point on an aircraft and divided by the mean aerodynamic chord, making them dimensionless. A dimensionless value eliminates unit conversions, simplifying calculations and comparisons. In this case, h and h_n are measured from the wing root leading edge.

The neutral point is related to the moment at the cg and static stability by the lift coefficient. Lift is represented as acting at the neutral point, and thus generates a moment about the cg. Lift and pitching moment are non-dimensionalized by:

$$C_L = \frac{L}{q\,S} \qquad (2.1,1)$$

$$C_m = \frac{M}{q\,S\,\bar{c}} \qquad (2.1,2)$$

where L and M are lift and pitching moment, respectively, q is the dynamic pressure, S the wing area, and $\bar{c}$ the mean aerodynamic chord. Thus, the moment generated by the lift is calculated in coefficient form by

$$C_m = C_L (h - h_n) \qquad (2.1,3)$$

It should be noted lift is rarely perpendicular to the mean aerodynamic chord, but the angles were assumed slight enough to make the small angle approximation, $\cos \alpha \sim 1$. It should also be noted that this equation is for the entire aircraft, thus C_L includes the contributions of individual aircraft components, such as the tail.

Differentiating equation (2.1,3) with respect to α yields the pitch stiffness, $C_{m\alpha}$

$$C_{m\alpha} = C_{L\alpha} (h - h_n) \qquad (2.1,4)$$

where $C_{L\alpha}$ is the lift-slope, or change in lift with respect to α.

2.2 POWER-ON NP

2.2.1 WHY AND HOW POWER SHIFTS THE NEUTRAL POINT

Power affects the neutral point two ways, aerodynamically and through the propeller normal force, N_p. The effect of the propeller normal force will be examined first.

A rotating propeller generates a force normal to the thrust and in the plane of propeller rotation. This force is known as the propeller normal force and its magnitude varies with α. The normal force is non-dimensionalized by

$$C_{Np} = \frac{N_p}{q S_p} \qquad (2.2,1)$$

where C_{Np} is the propeller normal force coefficient and S_p is the propeller disk area. The normal force acts in the upward direction in reference to the aircraft body, thus changing the aircraft pitching moment

$$\Delta C_m = C_{Np} \frac{l_p}{\bar{c}} \frac{S_p}{S} \qquad (2.2,2)$$

where l_p is the distance measured from the propeller to the aircraft cg.

To determine the C_{Np} contribution to pitch stiffness, the effect of the wing-induced upwash at the propeller must also be considered. Upwash at the propeller varies with α. This is denoted $d\varepsilon_p / d\alpha$. When the propeller is aft of the wing, i.e. a pusher-configuration, the propeller experiences wing-induced downwash. To indicate this, the value of $d\varepsilon_p / d\alpha$ is negative.

Differentiating equation (2.2,2) with respect to α and adding the upwash term yields

$$(C_{m\alpha})_{prop} = K (C_{Np})_\alpha \qquad (2.2,3)$$

$$K = \frac{S_p}{S} \frac{l_p}{\bar{c}} \frac{d\alpha_p}{d\alpha} \qquad (2.2,4)$$

$$\frac{d\alpha_p}{d\alpha} = \left(1 + \frac{d\varepsilon_p}{d\alpha}\right) \qquad (2.2,5)$$

where $(C_{m\alpha})_{prop}$ is the change in pitching moment due to the propeller with respect to a change in α, and K is the propeller wash coefficient. Note that when the propeller is forward of the cg, such as in a tractor-configured aircraft, l_p is positive, thus $(C_{m\alpha})_{prop}$ is positive and thus destabilizing. When the propeller is aft of the cg, such as in a pusher-configured aircraft, l_p is negative, thus $(C_{m\alpha})_{prop}$ is negative and stabilizing.

Values for $d\alpha_p/d\alpha$ are estimated in reference (10), and vary with aspect ratio, AR, and position relative to the wing quarter chord. The values range from 1.1 to 2.1 forward of the wing, and 0 to 0.6 aft of the wing[10].

Now consider the aerodynamic effects on power. Aircraft geometry, particularly location of the power source has a major impact on power effects. A rotating propeller generates a slipstream. The slipstream is a rotating airflow behind the propeller. Thus, where the engine is placed and the geometry of the surfaces affected will influence the way power effects the aircraft. The effect of the slipstream on the aircraft aerodynamics is complex and extremely difficult to accurately predict. Wind tunnel testing is commonly used to estimate the power effects. However, it is known that lifting surfaces in the slipstream, such as wings or tails, experience an increase in lift-slope[14].

The wing of a tractor-configured, aft-tailed, aircraft is directly in the slipstream. The tail is significantly further from the propeller, thus the effects of the slipstream on the tail lift-slope are less dramatic. For a pusher-configured aircraft, the wing is forward of the propeller and the tail is directly in the slipstream, thus the effects on the tail lift-slope are more pronounced.

How this affects the neutral point location can be seen by considering the individual contributions aircraft components make to the aircraft pitch stiffness. By considering equation (2.1,4) with the wing/body aerodynamic center substituted for the neutral point, the contribution of the tail and normal force must be expressed as separate terms.

$$C_{m\,\alpha} = C_{L\alpha}(h - h_{wb}) - (C_{L\alpha})_t V_H \left(1 - \frac{d\varepsilon_t}{d\alpha}\right) + (C_{m\alpha})_{prop} \qquad (2.2,6)$$

where h_{wb} is the wing/body aerodynamic center, $(C_{L\alpha})_t$ is the tail lift-slope, V_H is the tail volume ratio, and $d\varepsilon_t/d\alpha$ is the change in downwash at the tail with respect to changing α.

When the cg is at the neutral point, $C_{m\alpha}$ is zero (equation (2.1,4)). Applying this to equation (2.2,6) and re-arranging to solve for h_n yields

$$h_n = h_{wb} + \frac{(C_{L\alpha})_t}{C_{L\alpha}} V_H \left(1 - \frac{d\varepsilon_t}{d\alpha}\right) - \frac{(C_{m\alpha})_{prop}}{C_{L\alpha}} \qquad (2.2,7)$$

Now consider what is known about $(C_{m\alpha})_{prop}$ and the power effects on $C_{L\alpha}$ and $(C_{L\alpha})_t$.

For the pusher configuration, $(C_{m\alpha})_{prop}$ and slipstream effects on $(C_{L\alpha})_t$ both act to increase h_n, which is aft neutral point shift. This increases the static margin, which improves longitudinal stability. For the tractor-configuration $(C_{m\alpha})_{prop}$ and slipstream effects on $C_{L\alpha}$ result in a decrease in h_n, a forward neutral point shift. This decreases the static margin and reduces longitudinal stability.

2.2.2 ESTIMATION OF POWER-ON NP FROM FLIGHT DATA

The power-on neutral point was estimated from estimated aircraft weight, elevator deflection, δe, and q recorded during steady, level flight. The neutral point and elevator angle are related through C_m and C_L. Experience has shown aircraft lift and moment are approximated as aerodynamically linear in both δe and α[14,15].

$$C_L = C_{L\alpha}\alpha + C_{L\delta e}\delta e \qquad (2.2,8)$$

$$C_m = C_{mo} + C_{m\alpha}\alpha + C_{m\delta e}\delta e \qquad (2.2,9)$$

where C_{mo} is the pitching moment at zero α, α is measured with respect to the aircraft zero-lift line, and positive elevator deflection is taken as trailing edge downward.

By definition, the aircraft is trimmed when C_m equals zero. In steady, level flight, the aircraft is trimmed and the lift equals the weight. Equations (2.1,1), (2.2,8), and (2.2,9) become

$$C_{L\,trim} = \frac{W}{q\,S} \qquad (2.2,10)$$

$$C_{L\,trim} = C_{L\alpha}\alpha_{trim} + C_{L\delta e}\delta e_{trim} \qquad (2.2,11)$$

$$-C_{mo} = C_{m\alpha}\alpha_{trim} + C_{m\delta e}\delta e_{trim} \qquad (2.2,12)$$

Solving equations (2.2,11 and 12) for δe_{trim} yields

$$\delta e_{trim} = -\frac{C_{mo}C_{L\alpha} + C_{m\alpha}C_{L\,trim}}{C_{L\alpha}C_{m\delta e} - C_{L\delta e}C_{m\alpha}} \qquad (2.2,13)$$

By assuming there are no compressibility or aeroelastic effects, $C_{L\alpha}$ and C_{mo} can be considered constant. The low flight test speeds make the compressibility assumption valid. The original test vehicle was very rigid. Deviation as a result of aeroelasticity would be minimal and fall within an acceptable range of error. Unfortunately, that UAV was damaged during testing before data could be collected. The second UAV used to collect flight data was considerably less rigid, specifically its booms. However, the aeroelastic assumption was kept (and C_{mo} was still considered constant). The effect of boom flexing and this assumption is discussed later. C_{mo}, $C_{L\alpha}$, $C_{m\alpha}$, $C_{L\delta e}$, and $C_{m\delta e}$ were calculated by a CMARC analysis. CMARC is a fluid flow code discussed in section 2.6.

Substituting equation (2.1,4) into (2.2,13) and factoring out $C_{L\alpha}$ yields

$$\delta e_{trim} = -\frac{C_{mo} + [h - h_n]\,C_{L\,trim}}{C_{m\delta e} - C_{L\delta e}\,[h - h_n]} \qquad (2.2.14)$$

By definition

$$C_{m\delta e} = -C_{L\delta e} \frac{l_t}{\bar{c}} \tag{2.2,15}$$

where l_t is the distance from the tail aerodynamic center to the aircraft cg. Letting $\bar{l}_t$ equal the distance from the tail aerodynamic center to the neutral point, equation (2.2,15) becomes

$$C_{m\delta e} = -C_{L\delta e} \left[\frac{\bar{l}_t}{\bar{c}} + (h_n - h) \right] \tag{2.2,16}$$

Substituting equation (2.2,16) into equation (2.2,14) yields

$$\delta e_{trim} = \frac{C_{mo} + [h - h_n] C_{L\,trim}}{C_{L\delta e} \left(\frac{\bar{l}_t}{\bar{c}} \right)} \tag{2.2,17}$$

Figure 2.2 is a typical plot of δe_{trim} versus $C_{L\,trim}$[14]. Notice each static margin has the same y-intercept

$$\delta e_{C_{L\,trim\,zero}} = \frac{C_{mo}}{C_{L\delta e} \left(\frac{\bar{l}_t}{\bar{c}} \right)} \tag{2.2,18}$$

and the slope of each line is a function of the static margin. As the static margin increases, the slope of the line becomes more negative. Equation (2.2,18) was used to predict the y-intercept prior to flight-testing.

Taking the slope of the curves in Figure 2.2 or differentiating equation (2.2,18) with respect to $C_{L\,trim}$

$$\frac{d\delta e_{trim}}{dC_{L\,trim}} = \frac{[h - h_n]}{C_{L\delta e} \left(\frac{\bar{l}_t}{\bar{c}} \right)} \tag{2.2.19}$$

yields Figure 2.3 . From equation (2.2,19), the cg equals the neutral point at x-intercept, thus extrapolating the curve to the x-intercept yields the power-on neutral point estimate.

2.3 DETERMINATION OF POWER-OFF NP

Palindrome, a UAV, was designed to fly in two configurations, tractor and pusher, to yield two simultaneous equations. Except for the propeller and engine location, the UAV is identical in either configuration. The equations relate the power-off neutral point, h_n, to the power-on neutral point, $(h_n)_p$

$$(C_{m\alpha})_p = C_{m\alpha} + (C_{m\alpha})_{prop} \qquad (2.3.1)$$

where p indicates the power-on $C_{m\alpha}$.

Substituting equation (2.1,4) and (2.2,3) into equation (2.3,1) yields

$$C_{L\alpha}[h - (h_n)_p] = C_{L\alpha}(h - h_n) + K\,(C_{Np})_\alpha \qquad (2.3.2)$$

Dividing by $C_{L\alpha}$

$$[h - (h_n)_p] = [h - h_n] + \frac{K}{C_{L\alpha}}(C_{Np})_\alpha \qquad (2.3.3)$$

Consider equation (2.3,3) for each UAV configuration and there are two simultaneous equations with two unknowns, $(C_{Np})_\alpha$ and h_n. The solution of the power-off neutral point becomes trivial. The power effects on the neutral point are easily realized by comparing the power-off neutral point and the power-on neutral point estimated from flight data.

2.4 ESTIMATION OF POWER EFFECTS

Due to time constraints and flight-testing mishaps, flight data was only obtained for the tractor configuration. Thus, the solution of two simultaneous equations could not be used to estimate the power effects on the neutral point. The power-on neutral point was estimated as described in section 2.3. The CMARC predicted neutral point was assumed to be the power-off neutral point. The power effects were estimated by comparing the two.

To verify reasonable results where obtained, equation (2.3,3) was rearranged to solve for Palindrome's $(C_{Np})_\alpha$

$$(C_{Np})_\alpha = \left[h_n - (h_n)_p \right] \frac{C_{L\alpha}}{K} \qquad (2.4,1)$$

and compared to a typical $(C_{Np})_\alpha$ value of a single-engine, propeller-driven aircraft. Reference (16) estimates

$$\frac{dC_{m_{Np}}}{dC_L} = 0.02 \frac{l_p}{\bar{c}} \qquad (2.4,2)$$

for a single-engine World War II fighter. By definition,

$$\frac{dC_{m_{Np}}}{dC_L} = (C_{Np})_\alpha \frac{S_p}{S} \frac{l_p}{\bar{c}} \frac{d\alpha_p}{d\alpha} \frac{1}{C_{L\alpha}} \qquad (2.4,3)$$

Set the right hand sides of equations (2.4,1) and (2.4,2) equal

$$0.02 = (C_{Np})_\alpha \frac{S_p}{S} \frac{d\alpha_p}{d\alpha} \frac{1}{C_{L\alpha}} \qquad (2.4,4)$$

Solving for $(C_{Np})_\alpha$

$$(C_{Np})_\alpha = 0.02 \frac{S}{S_p} \frac{d\alpha}{d\alpha_p} C_{L\alpha} \qquad (2.4,5)$$

$C_{L\alpha}$ for a typical World War II single-engine fighter was estimated by

$$C_{L\alpha} = \frac{a_o}{1 + \frac{a_o}{\pi \, AR \, (1+\tau)}} \qquad (2.4,6)$$

where a_o is the two-dimensional lift slope and $(1+\tau) = e$. e is the Oswald efficiency factor[17]. The Oswald efficiency factor was estimated to be 0.90 based on the typical value range of 0.85-0.95[15]. The geometric values of the *Spitfire* vary significantly compared to Palindrome. The *Supermarine IX* was selected as a typical World War II single-engine fighter to use as a reference. Its aspect ratio is 5.60[18]. Thus, the *Spitfire's* $(C_{Np})_\alpha$ could be estimated.

2.5 AEROELASTIC (FLEXING) EFFECTS

Aeroelastic effects could be neglected in all regards, except one. Palindrome's tail/boom assembly was not rigid enough to rule out longitudinal effects due to flexing. The concern of longitudinal flexing is the change in C_{mo}.

$$C_{mo} = (C_{mo})_w + (C_{mo})_f + \eta V_H (C_{L\alpha})_t (\varepsilon_o + i_w + i_t) \qquad (2.5,1)$$

where $(C_{mo})_w$ and $(C_{mo})_f$ are the wing and fuselage contribution to C_{mo}, respectively, ε_o is the downwash at the tail at zero angle of attack, and i_w and i_t are the wing and tail incidence angle, respectively (i_t and i_w are referenced to the fuselage x-axis).

The wing and body terms of equation (2.5,1) are of no concern here due to the rigidity of these components. By design, i_w equals zero. To estimate the effect of flexing

on C_{mo}, the change flexing imposes on the effective angle of attack ($\alpha_{eff} = \varepsilon_o + i_t$) of the tail must be determined. Assuming small boom deflections, the change in i_t can be assumed linear with deflection. The change in downwash at the tail, $d\alpha_t/d\alpha$, is approximated as constant by utilizing methods in reference (10). Thus, the change in ε_o is linearly proportional to the change in α at the tail. The result is α_{eff} is linearly proportional to the deflection.

$$\Delta C_{mo\ flex} = \eta V_H \left(C_{L\alpha}\right)_t \left(\Delta\alpha_{eff}\right) \qquad (2.5,2)$$

The only variable in equation (2.5,7) that is not a constant is $\Delta\alpha_{eff}$. Thus, $\Delta C_{mo\ flex}$ was a linear function of $\Delta\alpha_{eff}$.

A change in C_{mo} changes $\delta e_{C_{L\ trim\ zero}}$ on Figure 2.2 (equation (2.2,18)) and δe_{trim} (equation (2.2,17)). Notice the slope of Figure 2.2 is not affected by a change in C_{mo}. The plot of Figure 2.2 simply shifts up or down a value proportional to the tail deflection. The neutral point is estimated from the slope of the curves in Figure 2.2. Thus, the shift will not affect the neutral point estimate.

To estimate the aeroelastic effect on $\delta e_{C_{L\ trim\ zero}}$, $\Delta C_{mo\ flex}$ was calculated for a $\Delta\alpha_{eff}$ of 5 degrees. From simple geometry, this corresponds to a 3-inch deflection of the tail. Three inches was chosen based on the deflections observed while handling the aircraft during flight preparation, etc. Typical values for η range from 0.8 to 1.2, depending on the tail location. For tails located in the wake of the wing, η is less than unity. η was estimated as 0.9. V_H is a ratio of aircraft geometric constants. $\left(C_{L\alpha}\right)_t$ was estimated using

equation (2.4,6) and the tail geometry. This yielded $\Delta C_{mo\ flex} = 0.1351$. From equation (2.2,18), this resulted in a $\delta e_{C_{L\ trim\ zero}}$ shift of 14.2 degrees.

2.6 CMARC ANALYSIS

CMARC is a low order panel method, fluid flow analysis code available from AeroLogic. It is a descendant of Analytical Methods' VSAERO and an enhanced version of NASA's PMARC-12.

CMARC analyzes three-dimensional surface models. The surfaces are divided into a large number of quadrilateral panels. CMARC recognizes a triangular panel as a quadrilateral panel with a side of length zero.

CMARC carries out a series of calculations, assuming irrotational, incompressible flow, to obtain the solution for the potential flow. From this, individual pressure coefficients are found for each panel. Each pressure coefficient is applied uniformly over its respective panel and the model's aerodynamic properties are calculated.

It has been shown this provides an acceptable level of accuracy compared to higher-order methods, when a dense enough panel distribution is used[19]. Special care was taken by the Palindrome design team to ensure a dense distribution was used during modeling, particularly in areas of steep pressure gradients, such as the leading edge of the wing.

CMARC was also used to estimate stability derivatives. Selected values from the CMARC analysis are presented in Table 2.1. A sample pressure distribution is displayed in Figure 2.4.

3 FLIGHT TESTING

3.1 INTRODUCTION

Flight-testing was conducted at NCSU's Perkins Field, in Butner, NC. It was to consist of two sets of flights, one set in tractor and the other in pusher. Each set consisting of a flight at 6%, a flight at 8%, and a flight at 10% static margin.

The Daedalus UAV was the first aircraft used in this project. On the first flight attempt the fuel tank was not adequately secured. The aircraft experienced a 2g acceleration for take-off, causing the fuel tank to go to the tail of the aircraft. The resulting cg shift caused Daedalus to be unstable and crashed on take-off.

The second UAV, Palindrome, had a successful set of flights in tractor configuration, but the first attempt in pusher resulted in substantial damage. Repair time was beyond time constraints of the project and it was decided to conclude the project with the data collected.

3.2 TEST VEHICLE

The Palindrome UAV was designed and constructed by eight members of the 2000-2001 North Carolina State University Aerospace Engineering Senior Design Class (MAE 478 and MAE 479). The UAV was required to satisfy customer requirements assigned with this research in mind (Table 3.1)[16].

Palindrome was designed to fly in either pusher or tractor configuration without changing the geometry of the aircraft. It is comprised of three main assemblies, the fuselage, the wing assembly, and the boom empennage. The boom empennage attaches to

the wing assembly, which attaches to the fuselage. Converting from tractor to pusher configuration is relatively simple. The fuselage is detached from the wing/empennage assemblies, turned around, and reattached. The only significant aerodynamic difference between the configurations is the propeller/engine location (Figure 3.1).

Customer requirements stated the O.S. Surpass III Four-Stroke Engine had to power the UAV. Palindrome's design team conducted an engine/propeller matching analysis to determine the best combination. The analysis was limited to propellers that were available from a single manufacturer in both the pusher and tractor configuration. This ensured symmetry and aerodynamic properties did not change between the two aircraft configurations. The 15 x 10 propeller was selected for its high efficiency at cruise, highest maximum velocity, and excess power at stall and cruise[16].

Palindrome lands on skids and is launched from a dolly catapulted down the runway by bungee cords. Skids are aerodynamically cleaner, simpler to design, and simpler to manufacture than landing gear. The bungee cords are attached to the dolly and the dolly is pulled back a predetermined distance by a winch. Palindrome sat on two posts on the launch dolly in a tandem configuration.

Just aft of the forward post is the release mechanism, which holds the UAV on the dolly until they reach a pre-determined release point. The release mechanism is a clamp like device that fastens around a U-bolt on the underside of the fuselage (Figure 3.2). It is held closed by two pins tied to a release line. The other end of the release line is tied to the winch. Enough line is let out so that the release pins will be pulled free at the take-off point.

When the pull back line was unleashed for Palindrome's first pusher flight, the release mechanism failed. By design, ninety percent of the weight rested on the rear post to create the ability to rotate for take-off[16]. The resulting pitching moment from the rear post of the dolly caused Palindrome to flip backwards off the dolly, land on its tail, and snap both booms. Both vertical surfaces were split open and the engine mounts failed. The engine skidded down the runway separated from its vehicle.

Palindrome flew three times in tractor configuration, before flight data was successfully obtained. Prior to each of these three flights, the avionics functioned properly, but no data was present when downloads were attempted. It was later determined the avionics ground wire had not been secured well enough. The impact of landing was just hard enough to temporarily separate the ground wire and the power bus, thus cycling power to avionics and erasing the data. To prevent a re-occurrence, all wiring was re-examined, and tightened. An impact and shake test was performed to test for loose connections.

3.3 DATA RECORDING

A Flight Computer System (FCS) was used with the program servo.hex to record elevator deflection commands and dynamic pressure during flights[17]. The elevator command signal from the on-board receiver was sent to both the FCS and the servo. The FCS recorded the dynamic pressure via a pitot-static tube and pressure transducer. A pilot actuated switch on the transmitter enabled data recording only during the desired flight condition, steady, and level. This simplified post flight data reduction. Data recorded at

each actuation of the switch is referred to as a (data) collection set. The FCS recorded data as a sixteen-bit integer.

Steady, level flight was estimated by constant throttle position and visually. Low altitude, high-speed passes were visually easier to estimate and thus more accurate. The runway provided an easy reference to determine level flight, but the number of high-speed, low altitude passes was limited by flight safety. Higher altitude, low speed passes were more difficult to accurately estimate level flight without the runway as a reference.

3.4 ELEVATOR DEFLECTION

Prior to flights, a calibration was performed relating the elevator position to the transmitter elevator command. A mirror was attached to the elevator and a laser was positioned to reflect off the mirror onto a chalkboard. At twenty-six elevator positions, a mark was made where the laser reflected on the chalkboard and the FCS recorded the bit count. The elevator angle was determined from the simple geometry of the set-up (Figure 3.3).

The first data point was taken with the elevator near the middle of its range of motion. The elevator was then cycled directly to its minimum deflection, its maximum deflection, and back to the midpoint, only stopping at those three points. Data was recorded at each point. The elevator was again cycled to its minimum deflection, maximum deflection and back to the midpoint, but it was stopped at several points along the way and data was recorded. The order of data points recorded can be seen in Figure 3.4.

A plot of elevator angle versus a number proportional to the commanded servo position showed a linear fit best described the relationship (Figure 3.5). The points at the minimum deflection were excluded from the curve fit due to a mechanical limitation on elevator deflection.

3.5 DYNAMIC PRESSURE

The design team used CMARC predicted velocities to determine pitot-static tube placement. The difference in the local wing velocity and the freestream velocity are shown in Figure 3.6. To maintain symmetry of the aircraft, a dummy pitot tube was placed in the same location in the other wing.

The dynamic pressure from the pitot-static tube was measured by a pressure transducer in inches water. The pressure transducer output an analog signal proportional to dynamic pressure's magnitude, which was converted by an analog to digital converter board in the FCS. The inches water to analog voltage relationship was obtained from the transducer manufacturer data sheet.

Just before each take-off, the analog to digital converter was calibrated. A zero reading of the transducer was recorded with a cover placed over the pitot-static tube to eliminate any wind interference. The FCS recorded four more values corresponding to onboard calibration voltages. The five recorded values were used to determine the linear analog to digital conversion. Combining this relationship with the analog voltage to inches of water relationship, and converting from inches of water to Pascals, the integer to pressure relationship was plotted in Figure 3.7. The calibrations for Palindrome were

identical, thus only one was plotted. Dynamic pressure was converted to Pascals to eliminate later conversions and simplify calculations involving dynamic pressure.

3.6 SETTING THE STATIC MARGIN

Prior to each flight, the aircraft was hung with a rig to determine the center of gravity (Figure 3.8). The payload was secured in the vehicle and was not moved between the center of gravity tests and flight-testing. The fuel tank was centered at the 8% static margin cg location to minimize the cg shift resulting from fuel consumption.

The most fuel used for any flight was 0.15 lbs, or 0.68% of the total aircraft weight. Thus, the fuel cg needed to be a large distance from the required aircraft cg for fuel consumption to have a significant effect. The difference between the 8% static margin cg location and the 6% or 10% cg location was only 0.25 inches, or less than 0.5% of the aircraft length. Fuel consumption resulted in a 0.0057-inch cg shift, or a 0.04% static margin shift. Fuel consumption's effect on cg location and static margin was negligible.

To prescribe a specific static margin, the fulcrum of the rig was positioned over the desired cg location. A digital level indicated when the plane was balanced (i.e. the aircraft was properly balance when it was completely level). Lead shot in a foam container was used as ballast. Adding or removing ballast shifted the cg of the aircraft to the desired location. Once the aircraft was balanced for a particular static margin, the required ballast was removed and marked for flight-testing. The procedure was repeated for each static margin.

Using pre-packaged ballast from the cg test decreased turn around time at the airfield. After a flight, data was downloaded to a laptop computer. The plane was weighed then re-fueled. The appropriate ballast package was loaded and the aircraft was weighed again. The UAV was ready for flight.

3.7 IN FLIGHT WEIGHT ESTIMATION

Palindrome was not equipped with a fuel flow meter that would enable estimation of the exact aircraft weight for a given data collection set. The weight was estimated by assuming a constant rate of fuel usage throughout the flight and recording the engine run time and time each data collection set was recorded. Pre-flight, post-flight, and estimated aircraft weights are in Table 3.2.

4 RESULTS AND DISCUSSION

4.1 DATA PROCESSING

Each collection set was initially averaged. At the end and/or beginning of several collection sets there was a small amount of data that was not representative of steady, level flight. It was initially believed data had been recorded as the aircraft was approaching or exiting steady, level flight. The few "errant" values were not included in the averaging.

This did not produce the expected results (Table 4.1 and Figure 4.1 and 4.2). The y-intercept was predicted to be zero degrees elevator deflection, the same for each static margin, and the $d\delta e_{trim}/dC_{L\,trim}$ plot could not be reasonably assumed linear. However, the linear assumption was made to provide a comparison for the estimated power effects obtained from the following data processing approach.

After examining plots of δe_{trim} and q versus time (Figure 4.3), it was observed that a significant portion of any given collection set was not steady, level flight. Criteria were established to deem data as steady, level flight by examining time plots, and the data files. A range of one-degree elevator deflection and three miles per hour over a period of at least one second was deemed steady, level flight. This will be discussed momentarily. Data strings fitting the criteria were termed "steady state data strings". A sample steady state data string can be seen in Figure 4.4.

Also note on Figure 4.4 the oscillation to the right of the graph has a peak to peak value of roughly 0.1 degrees around –10.75 degrees. Recall from Figure 3.5 a 0.11degree

change corresponds to one count change recorded by the digital FCS system. This indicates the actual elevator angle was likely between the two peak values, and the digital value oscillated back and forth due to timing measurements of the input signal.

Due to environmental factors, such as the input signal, unsteadiness in the pilots hand, small changes in wind, etc., the expectation of sustained truly steady level flight with a change of only one count (or 0.11 degrees elevator deflection) is unreasonable. Even this oscillation was not maintained for a full second. If the range of elevator motion considered steady level flight was not expanded, it would be nearly impossible to collect flight data.

Another indicator of whether this was stringent enough criteria, is low amount of recorded flight data actually used. Of the approximately 63 seconds of flight data recorded, only 20 seconds was used. This means that only 32% of what was visually deemed steady, level flight, met the steady state data criteria. This particular estimate does not guarantee the data was actually steady, level flight, but it can be used as an indicator.

With criteria established, the collection sets were examined for steady state data strings. Eight of the eighteen collection sets did not contain an acceptable data string. However, four of the collection sets contained at least two and as many as four acceptable data strings. A total of seventeen “steady state” data strings where averaged. This method produced results closer to what was expected (Table 4.2 and Figure 4.5 and 4.6).

Examining Figure 4.6 , a linear fit to the plot can reasonably be assumed. However, the y-intercepts still where not equal to the predicted value. Their range was reduced from just under ten degrees from the averaged data to less than four degrees for

the steady state data. The y-intercept predicted from CMARC values was zero degrees. The largest variation from the predicted intercept was 10 degrees. Recall from the aeroelastic effect estimation the shift was predicted to be 14.2 degrees. This combined with the linear assumptions made about the aeroelastic effects, implies the boom/tail deflection was less than 3-inches and the only significant aeroelastic effect was the y-intercept shift.

4.2 ESTIMATED POWER EFFECTS ON THE NEUTRAL POINT

The estimated power effect on the neutral point from simple averaging was 0.062 forward, or 6.2%. If this were a valid estimate, the power effects would have caused a negative static margin for the 6% static margin flight, making the aircraft longitudinally unstable. At best, the aircraft would have impossible for the pilot to control. The aircraft did not exhibit longitudinal instability. This result is clearly not valid.

While the magnitude of the estimated power effect on the neutral point was not valid, the direction of the neutral point shift was. The neutral point shifted forwarded, as expected for the tractor-configuration, indicating the power effect estimate was on the right track.

The estimated power effect using the steady state approach was a more reasonable 0.045 forward, or 4.5% (Table 4.3). The direction of the shift was once again as expected. The magnitude of the neutral point shift reduced the static margin by 75% of its original value for the 6% static margin flight and 56% for the 8% static margin flight. This offers an explanation for the less than desirable response to elevator deflection observations

made by the design team and pilot. By the steady state estimate above, the power-on neutral point shift reduced the power-on static margin to only 1.5% and 3.5%, for the 6% power-off static margin and 8% power-off static margin flights, respectively.

4.3 $(C_{Np})_{\alpha}$

$(C_{Np})_{\alpha}$ was estimated for Palindrome and a *Supermarine Spitfire IX*. To calculate Palindrome's $(C_{Np})_{\alpha}$, K, which is a function of $d\varepsilon_p/d\alpha$, was first calculated. An estimate for $d\varepsilon_p/d\alpha$ for Palindrome was obtained from reference (10). To ensure any inaccuracies that may have been present in the $d\varepsilon_p/d\alpha$ estimate did not have significant impact, the estimate was allowed to vary fifty percent. A fifty percent variation in $d\varepsilon_p/d\alpha$ yielded only a 4.5% change in K and a 4.7% change in $(C_{Np})_{\alpha}$. K was calculated to be 0.504. Palindrome's $(C_{Np})_{\alpha} = 0.611$.

To accurately estimate $(C_{Np})_{\alpha}$ for the *Supermarine Spitfire IX*, a World War II fighter, the *Spitfire's* $C_{L\alpha}$ was calculated to be 4.497. Geometric data for the *Spitfire's*, $d\alpha_p/d\alpha$, and S_p were obtained from reference (18) and is in Table 4.3. $(C_{Np})_{\alpha}$ for the *Spitfire* was estimated to be 0.732.

$(C_{Np})_{\alpha}$ for both aircraft are on the same order and differ by 20% of Palindrome's estimated $(C_{Np})_{\alpha}$. $(C_{Np})_{\alpha}$ values on the same order and relatively close, implies the power effect estimation was reasonable. The $(C_{Np})_{\alpha}$ difference is likely a result of the aircraft geometries, engines, and propellers.

5 CONCLUSIONS AND RECOMMEDATIONS

5.1 CONCLUSIONS

Two approaches for the estimation of power effects on the neutral point of a UAV were explored, the solution of two simultaneous equations and comparing computer code predictions with flight data estimations. The solution of two simultaneous equations approach was stopped short of completion due to flight-testing mishaps and time constraints.

The second approach, comparison of the CMARC predicted power-off neutral point to the flight data estimated power-on neutral point did not produce precisely the anticipated results. However, the comparison did show a reduction in stability in the form of a forward shift of the neutral point for the tractor configuration and estimates of $(C_{Np})_{\alpha}$ and power effects on the neutral point.

These estimates are of interest to designers in the areas of longitudinal static stability and controls, particularly designers of UAVs with similar propellers/engines and/or geometries to Palindrome. The estimates can be used to aid in sizing and placement of longitudinal controls surfaces (such as elevators or elevons) to overcome the destabilizing effects of the tractor configuration and provide adequate stability.

5.2 RECOMMENDATIONS

Future testing should be conducted to complete the solution of simultaneous equations. Solving the equations will yield the true power-off neutral point. This will

provide a comparison for CMARC predicted power-off neutral points and better estimations of power effects and $(C_{Np})_{\alpha}$. Future research should also consider improved ways to estimate steady, level flight, and consider the effects of flexing prior to flight.

The approaches taken here should also be expanded to other UAVs, leading to a wider selection of experimental data for future designers to refer to for power effect estimates. The engine placement and aircraft geometries that influence the flow into the engine have an impact on the power effects on the neutral point. Once a large amount of estimates are made for various geometry configurations and power plants, a single reference source should be compiled to provide a quick guide to make power effect estimations during design. Designers would base their power effect estimates on geometry and power configurations of the UAV. With a large enough base of experimental data, a future study should develop and validate a comprehensive theory to predict the power effects on the neutral point of a UAV (or aircraft). The development of the reference source and/or a comprehensive predictive theory will reduce the need for expensive wind tunnel testing.

6 REFERENCES

[1] Garamone, Jim; "From the US Civil War to Afghanistan – a Short History of UAVs" Army Communicator On-line, Vol. 27, No. 2, Summer 2002. Internet, 2 October 2003, available from http://www.gordon.army.mil/AC/sumr02/uav2.htm

[2] Public Broadcasting Service; "NOVA: Spies that Fly" Internet, 2 October 2003, available from http://www.pbs.org/wgbh/nova/spiesfly/uavs.html

[3] National Aviation Hall of Fame; :Enshrinee List" Internet, 2 October 2003, available from http://www.nationalaviation.org/museum_enshrinee.asp?eraid=2&enshrineeid =277

[4] Edwards Airforce Base Flight Test Museum; "Unmanned Aerial Vehicles" Internet, 15 October 2003, available from http://www.edwards.af.mil/articles98/docs_html/splash/ may98/cover/early.htm

[5] Jones, Christoper A.; "Unmanned Aerial Vehicles (UAVS) an Assessment of Historical Operations and Future Possibilities," Research Paper, Air Command and Staff College, March, 1997.

[6] Federation of American Scientists: "RQ-1 Predator MAE UAV" Internet, 15 October 2003, available from http://www.fas.org/irp/program/collect/predator.htm

[7] United States Navy: "F/A-18E/F *Super Hornet*," Fact File, Internet, 6 October 2003, available from http://www.chinfo.navy.mil/navpalib/factfile/aircraft/air-a18super.html

[8] Federation of American Scientists: "Medium Altitude Endurance UAV, Predator," Advanced Concept Technology Demonstrations Master Plan, Internet, 6 October 2003, available from http://www.fas.org/spp/military/docops/defense/actd_mp /MAE.htm

[9] Shephard's; " Unmanned Vehicles Handbook-The International Guide to the Unmanned Vehicles Industry," The Shepard Press, Burnham, Bucks, England 2002.

[10] Ribner, H. S.: "Notes on the Propeller and Slipstream in Relation to Stability," NACA Report L-25, October 1944.

[11] Weil, Joseph; Sleeman, Jr., William C.: "Prediction of the Effects of Propeller Operation on the Static Longitudinal Stability of Single-Engine Tractor Monoplanes with Flaps Retracted," NACA Report 941, 1949.

[12] White, Maurice D.: "Estimation of Stick-Fixed Neutral Points of Airplanes," NACA Report L-116, 1945.

[13] Goett, Harry J.; Pass, H. R.: "Effects of Propeller Operation on the Pitching Moments of Single-Engine Monoplanes," NACA Report L-761, May, 1941.

[14] Etkin, Bernard; Duff Reid, Lloyd: "Dynamics of Flight: Stability and Control," 3rd ed. John Wiley & Sons, Inc., New York, NY 1996.

[15] Nelson, Robert C.: "Flight Stability and Automatic Control," 2nd ed. McGraw-Hill, New York, NY 1998.

[16] Perkins, Courtland D.; Hage, Robert E.: "Airplane Performance Stability and Control," John Wiley & Sons, Inc., New York, NY 1949.

[17] Anderson, John D.: " Fundamentals of Aerodynamics," 2nd ed. McGraw-Hill, Inc., New York, NY 1991.

[18] Bridgman, Leonard: "Jane's All the World's Aircraft," The MacMillian Company, New York, NY August, 1944.

[19] AeroLogic: "Digital Wind Tunnel CMARC – User's Manual," AeroLogic, 2000.

[20] Palindrome Spring Report, North Carolina State University, Spring 2001.

[21] Heinzen, Stearns N.: " In-Flight Application of Active Separation Control Using Pulsed Jet Blowing," MS Thesis, North Carolina State University, 2000.

TABLES

Table 2.1: Sample CMARC Analysis Values

	6% Static Margin	8% Static Margin	10% Static Margin
$C_{L\alpha}$	4.963	4.963	4.963
$C_{L\delta e}$	0.184	0.184	0.184
C_{mo}	0.0008	0.0008	0.0008
$C_{m\alpha}$	-0.298	-0.397	-0.496
$C_{m\delta e}$	-0.565	-0.576	-0.587

Table 3.1: Palindrome Customer Requirements

Palindrome Customer Requirements	
Tractor/Pusher Configuration	Load Factors: +4g, -2g
$800 Budget	Land in 8 knot crosswind
Cruise > 75 mph	Dolly/Catapult launch
Stall < 35 mph	O.S. Surpass III Four-Stroke Engine
15 min Endurance at Full Throttle	No canards
Excellent Handling Characteristics*	Easily Transported by Students
Variable Static Margin	

*Defined as level 1 in Flying Qualities of Piloted Vehicles, USAF.

Table 3.2: Fuel Consumption

6% Static Margin		8% Static Margin		10% Static Margin	
Time (sec)	**Weight (lbs)**	**Time (sec)**	**Weight (lbs)**	**Time (sec)**	**Weight (lbs)**
Pre-Flight	22.20	Pre-Flight	22.70	Pre-Flight	23.35
246	22.14	254	22.62	233	23.28
359	22.10	346	22.59	269	23.27
394	22.09	363	22.59	274	23.27
395	22.09	364	22.59	276	23.27
474	22.06	372	22.58	278	23.27
478	22.06	Post-Flight	22.55	306	23.26
Post-Flight	22.05			Post-Flight	23.25
Engine Run Time (min:sec)	**Total Fuel Used (lbs)**	**Engine Run Time (min:sec)**	**Total Fuel Used (lbs)**	**Engine Run Time (min:sec)**	**Total Fuel Used (lbs)**
8:49	0.15	7:00	0.15	5:56	0.10

Table 4.1: Data Averaging Results

Flight 6% SM

Dyn Press (Pa)	mph	ft/sec	Elev Def (deg)	CL trim
285.05	48.48	71.11	-10.61	0.4614
351.30	53.82	78.94	-13.46	0.3742
568.64	68.48	100.43	-11.96	0.2315
676.24	74.67	109.52	-11.87	0.1946
867.63	84.58	124.06	-11.81	0.1518
881.54	85.26	125.05	-11.49	0.1496

Flight 8% SM

Dyn Press (Pa)	mph	ft/sec	Elev Def (deg)	CL trim
327.43	51.96	76.21	-15.42	0.4110
505.32	64.55	94.67	-10.70	0.2664
716.84	76.88	112.76	-11.68	0.1878
911.01	86.67	127.12	-10.93	0.1479
1194.57	99.25	145.56	-14.27	0.1128

Flight 10% SM

Dyn Press (Pa)	mph	ft/sec	Elev Def (deg)	CL trim
451.66	61.03	89.51	-16.90	0.3070
579.73	69.14	101.41	-14.08	0.2391
586.31	69.53	101.98	-12.31	0.2365
731.05	77.64	113.87	-10.59	0.1897
786.70	80.54	118.13	-10.67	0.1765

Table 4.2: Steady State Averaging Results

Flight 6% SM

Dyn Press (Pa)	mph	ft/sec	Elev Def (deg)	CL trim
326.16	51.86	76.06	-13.62	0.0906
399.90	57.42	84.22	-13.28	0.0739
562.41	68.10	99.88	-12.99	0.0526
669.30	74.29	108.96	-11.76	0.0442
686.58	75.24	110.36	-11.25	0.0431
872.16	84.80	124.38	-11.23	0.0340

Flight 8% SM

Dyn Press (Pa)	mph	ft/sec	Elev Def (deg)	CL trim
216.24	42.23	61.93	-17.44	0.1399
369.51	55.20	80.96	-12.17	0.0819
419.01	58.78	86.21	-12.56	0.0722
505.32	64.55	94.67	-10.70	0.0599
898.08	86.05	126.21	-10.30	0.0337

Flight 10% SM

Dyn Press (Pa)	mph	ft/sec	Elev Def (deg)	CL trim
315.16	50.98	74.77	-19.81	0.0989
321.97	51.53	75.57	-18.93	0.0968
448.06	60.78	89.15	-18.45	0.0696
448.06	60.78	89.15	-18.29	0.0696
586.20	69.52	101.97	-13.92	0.0531
1176.22	98.48	144.44	-15.40	0.0265
1492.21	110.93	162.69	-10.67	0.0209

Table 4.3: Power Effects and $(C_{Np})_{\alpha}$ Estimation Results

	Palindrome	**Spitfire**
Sp/S	0.1527	0.423
$(C_{Np})_{\alpha}$	0.611	0.732

Power Effects	
Simple Avg	0.062
Steady State	0.045

FIGURES

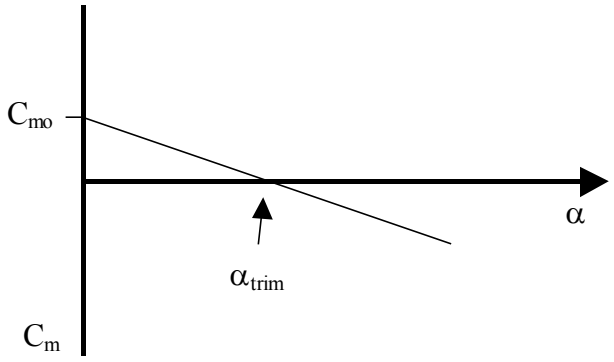

Figure 2.1: Static Stability

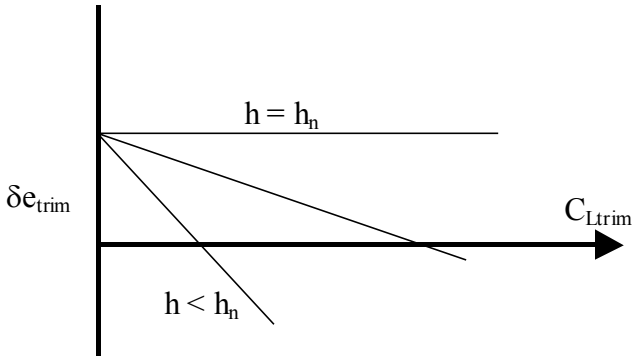

Figure 2.2: Typical Elevator Trim Angle

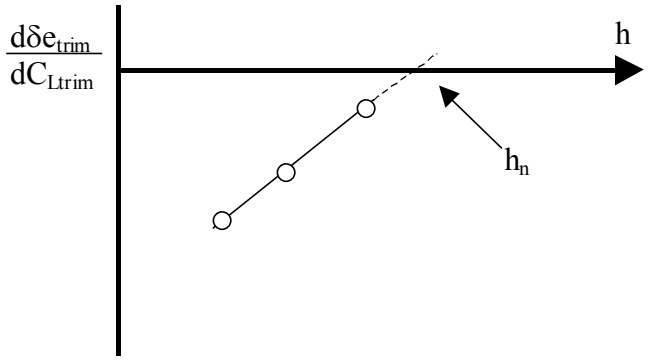

Figure 2.3: Estimation of Neutral Point

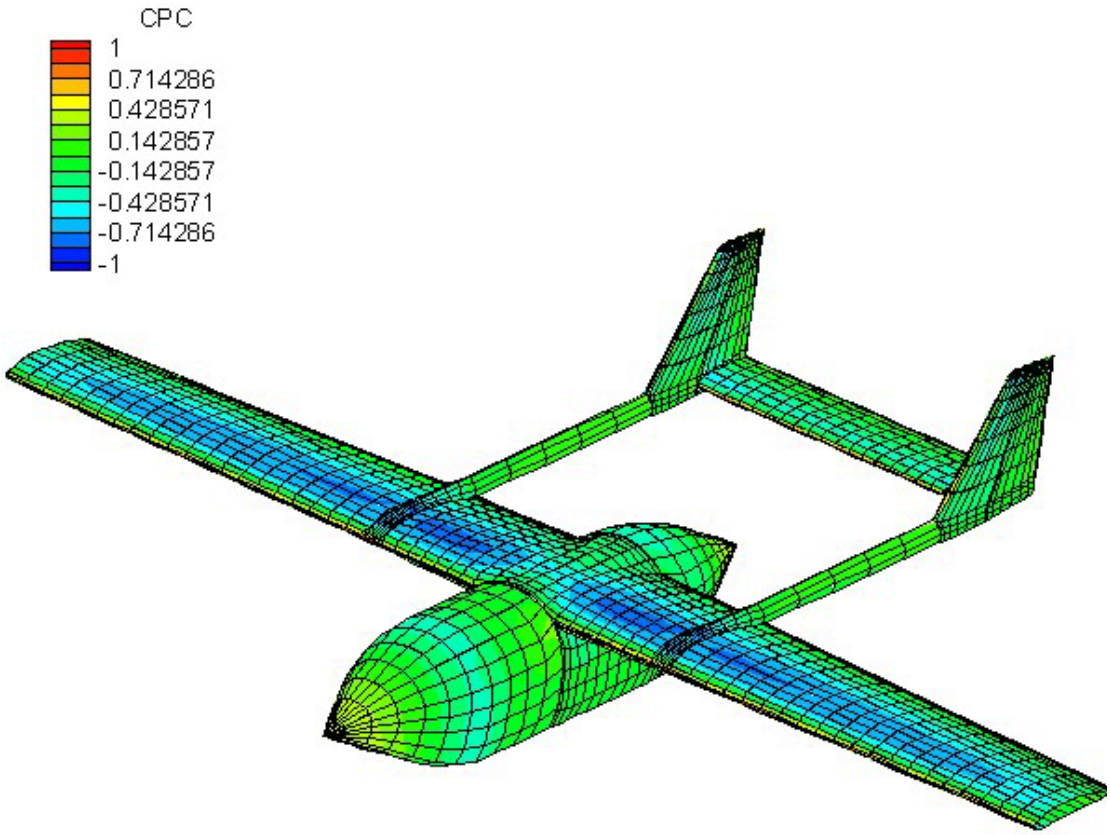

Figure 2.4: CMARC Baseline Run
(Reference 16)

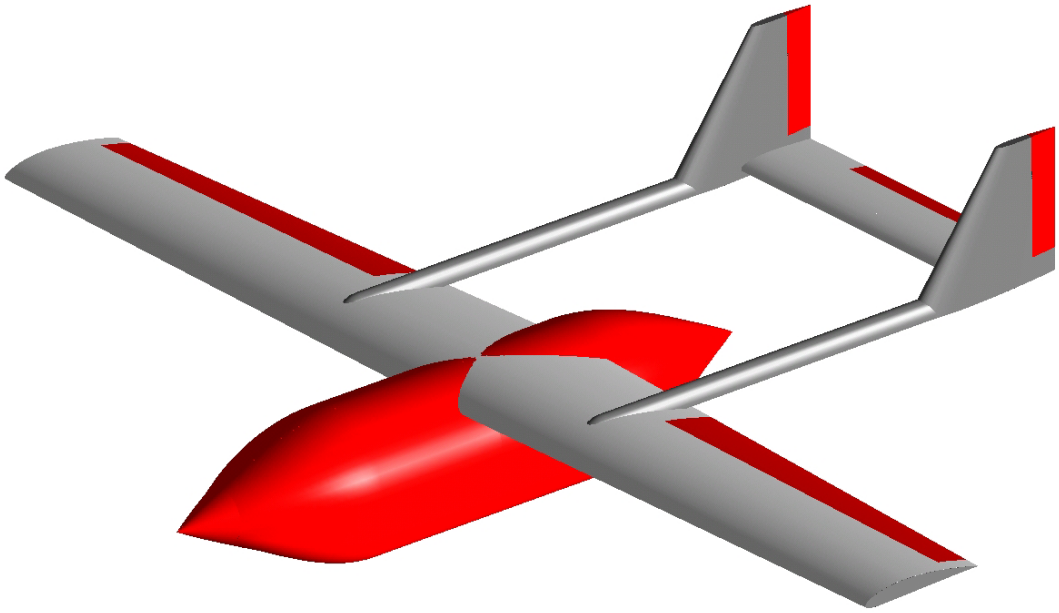

(a)

(b)

Figure 3.1: Palindrome

(a) Computer model of Palindrome. (b) Palindrome at Perkins Field in tractor. Notice the Fuselage is symmetric.

Figure 3.2: Release Mechanism

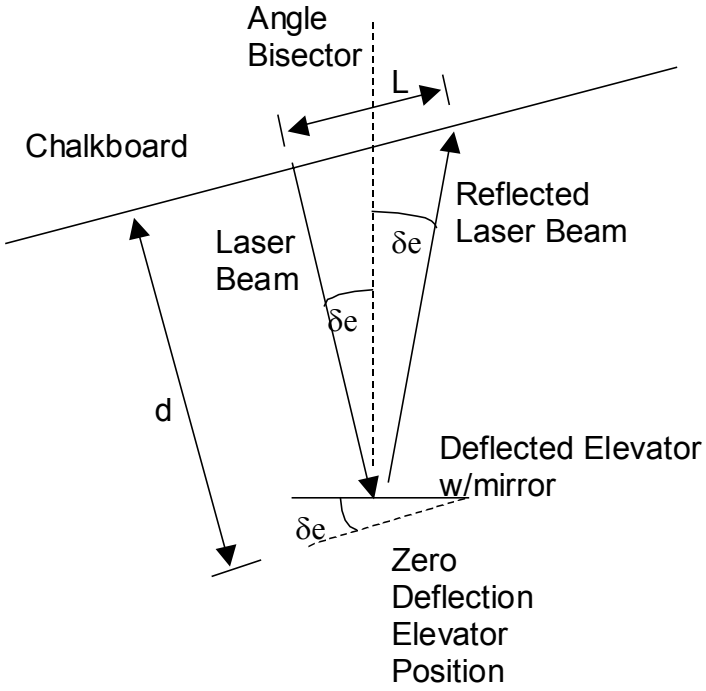

$\delta e = \tan (L/2d)$

Figure 3.3: Elevator Calibration Set-Up

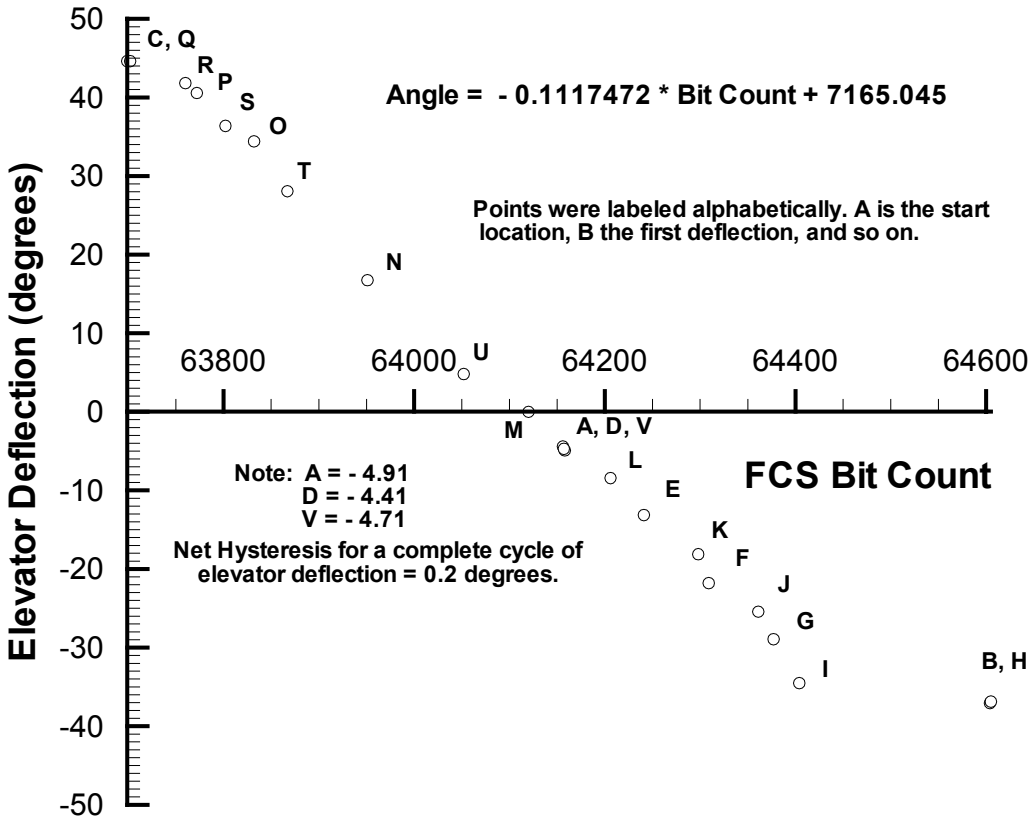

Figure 3.4: Elevator Calibration Data Point Progression

(Downward deflection taken as positive)

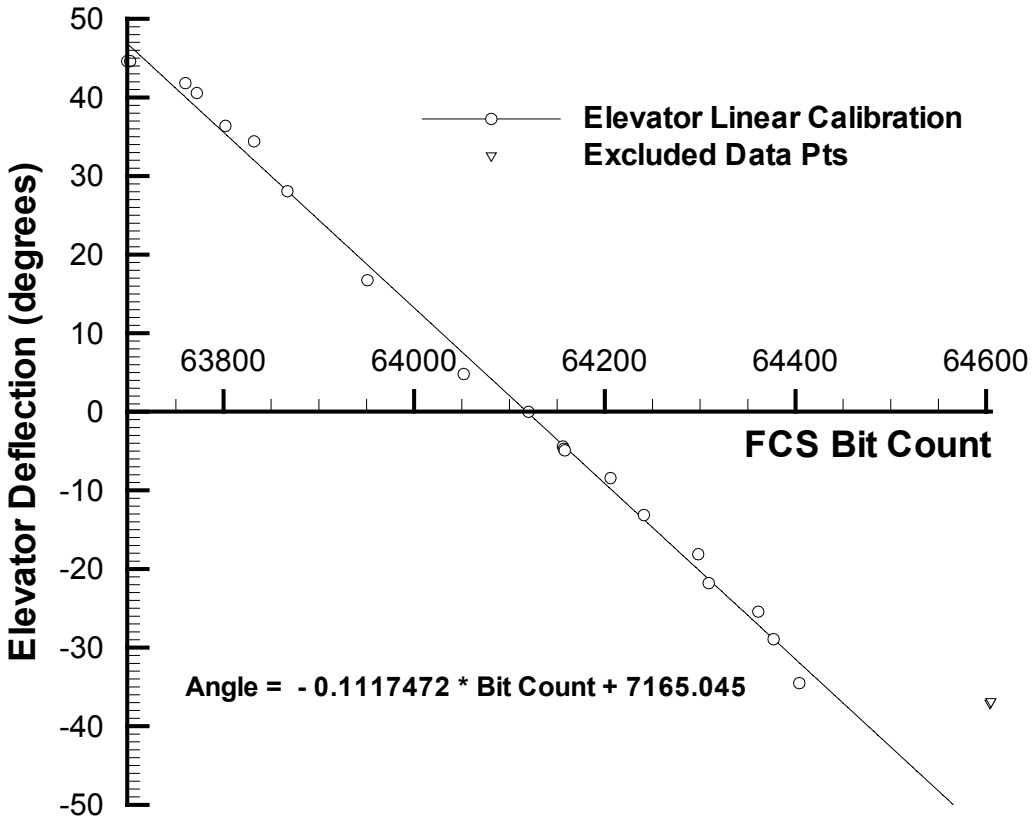

Figure 3.5: Elevator Calibration
(Downward deflection taken as positive)

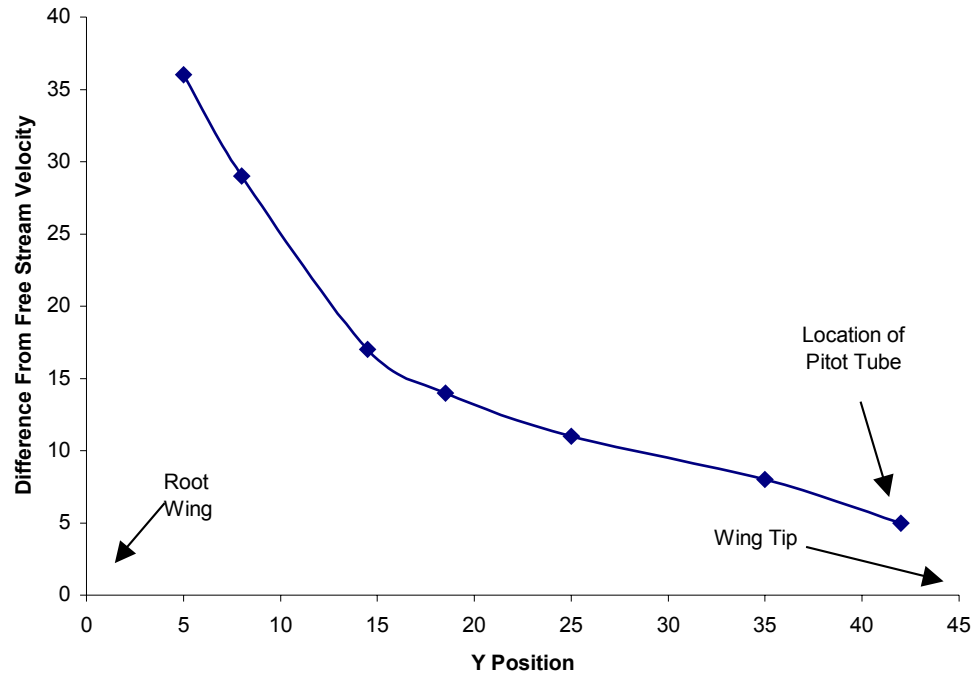

(a)

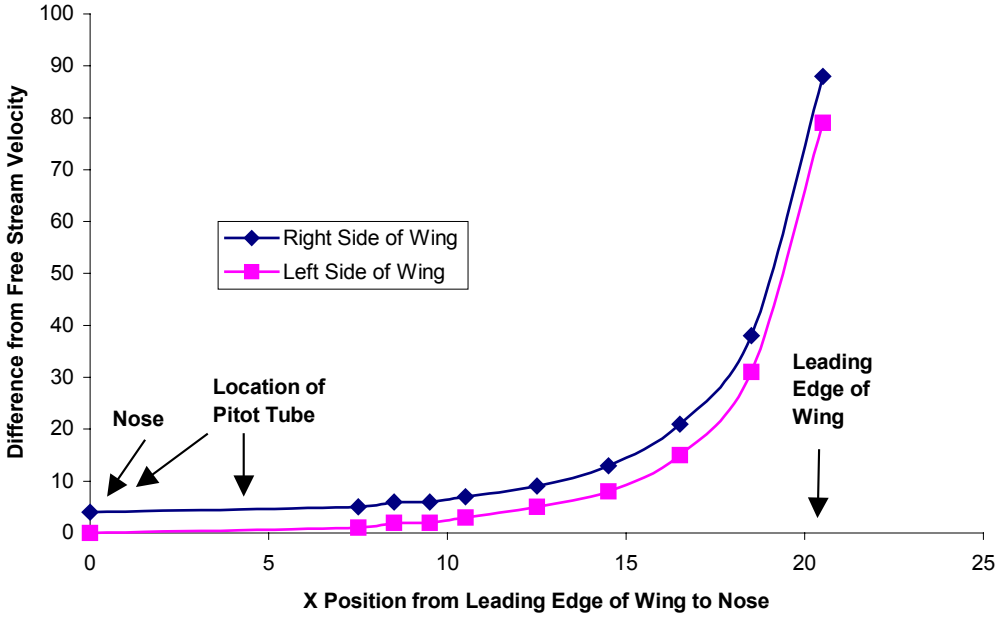

(b)

Figure 3.6: Difference in Freestream and Local Velocity for Pitot Placement

(Reference 16)

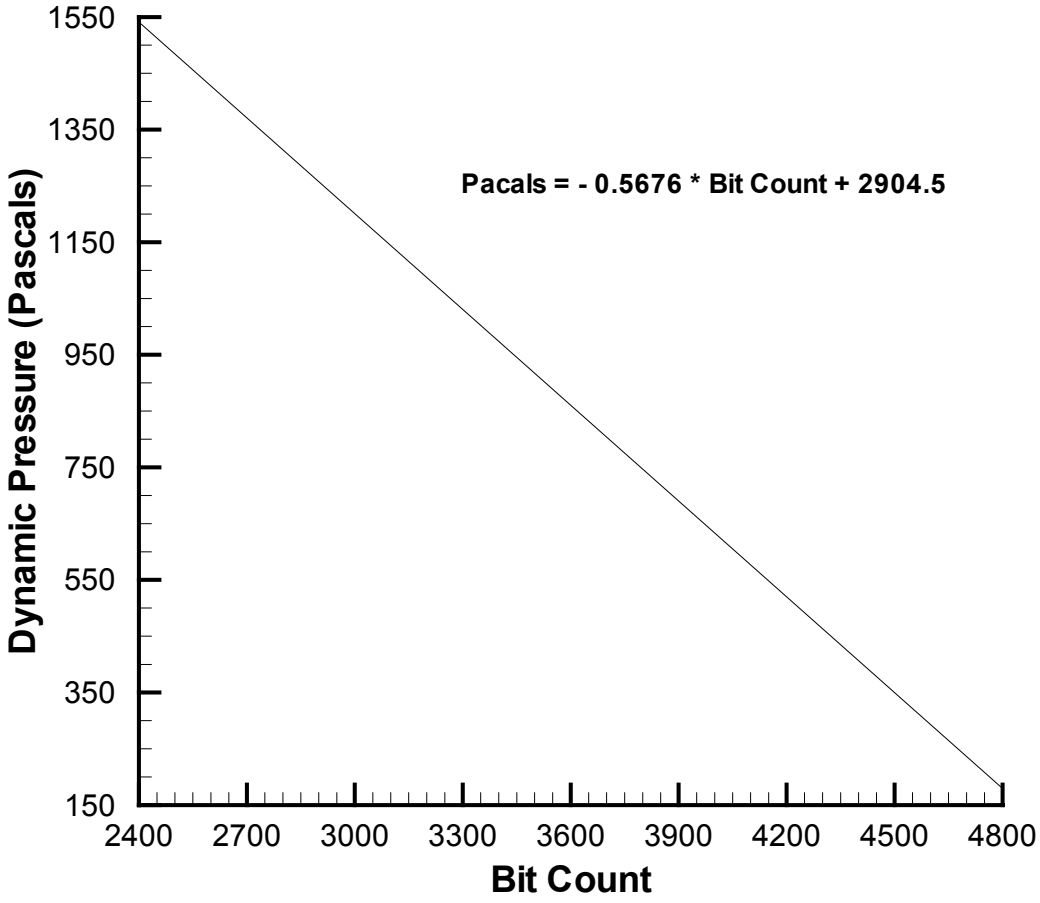

Figure 3.7: Transducer Dynamic Pressure Voltage Relationship

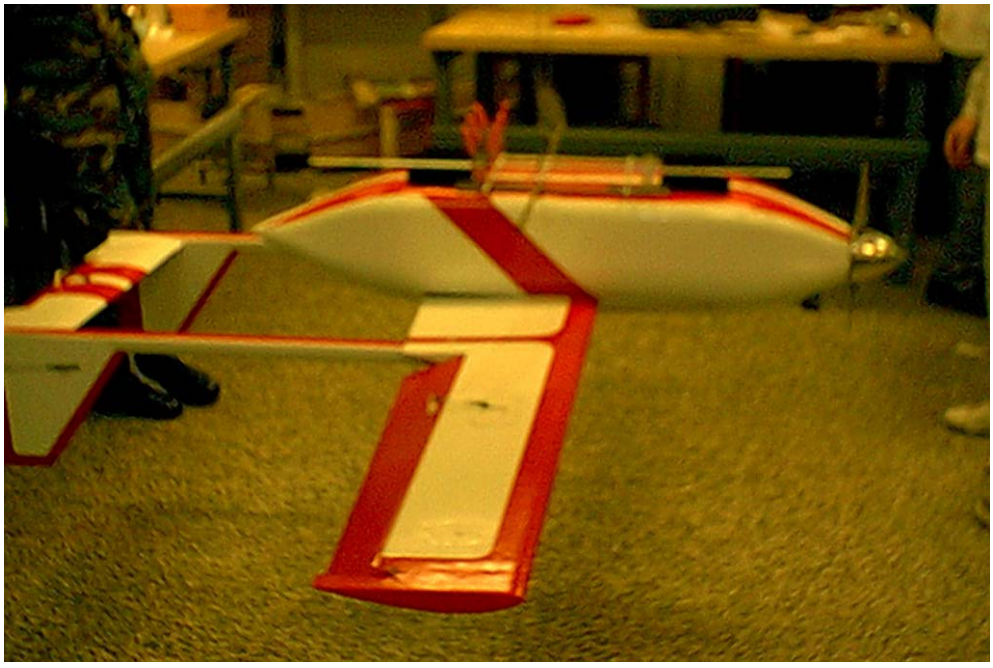

Figure 3.8: Center of Gravity Test
(Reference 16)

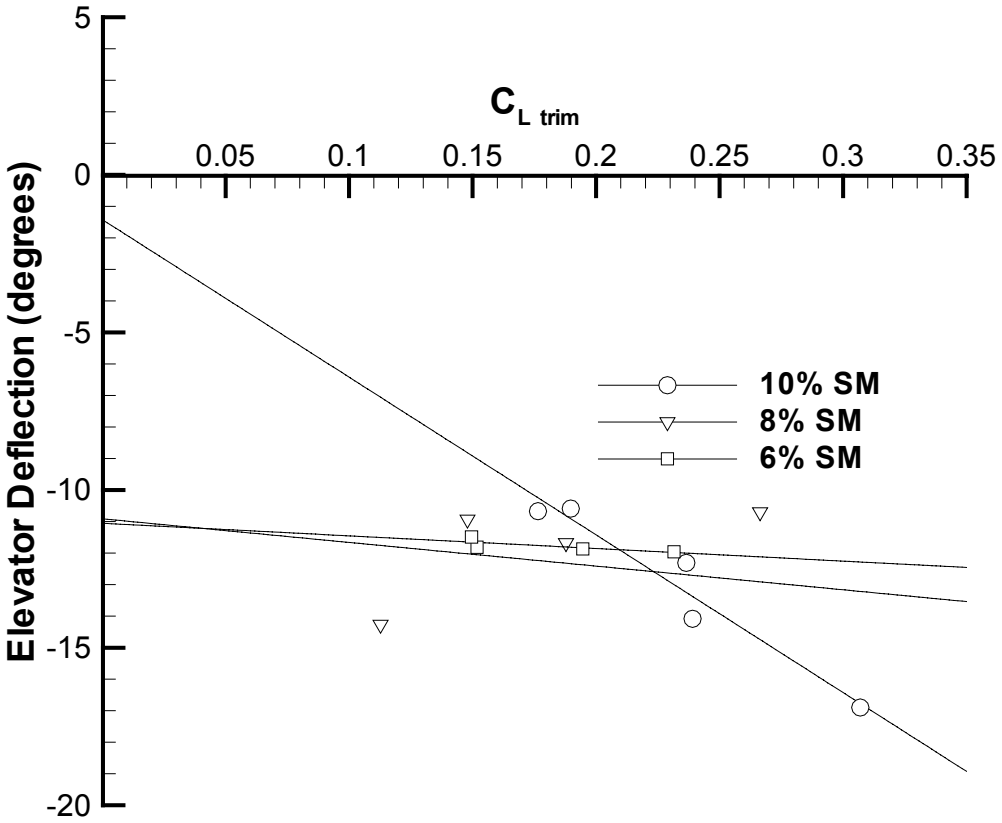

Figure 4.1: Data Averaging Results
(Downward deflection taken as positive)

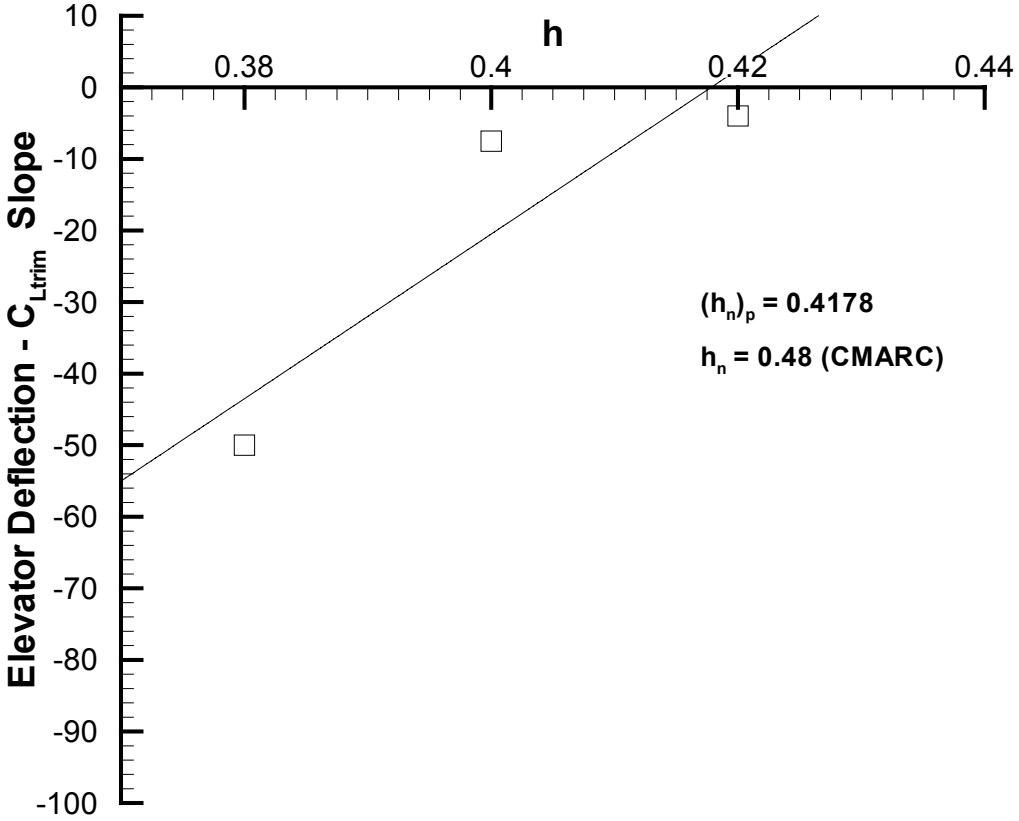

Figure 4.2: Data Averaging NP Results

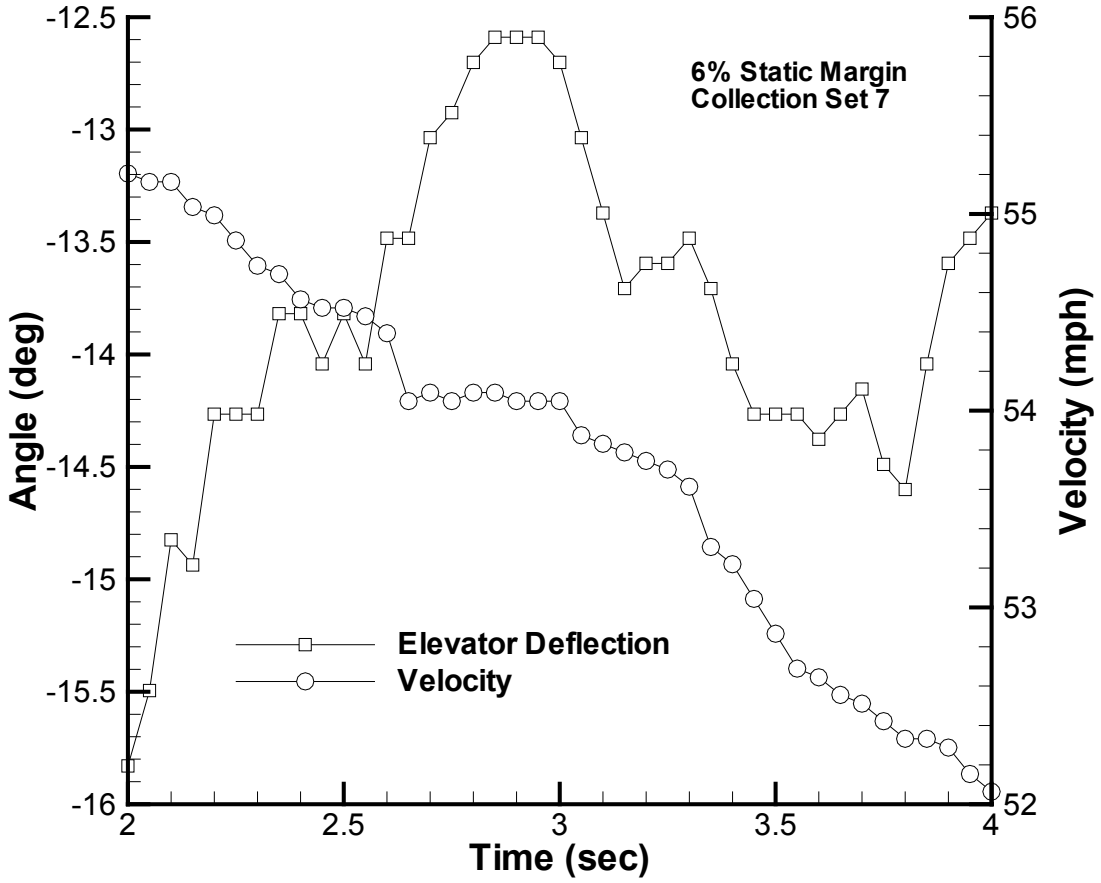

Figure 4.3: Undesirable Flight Data

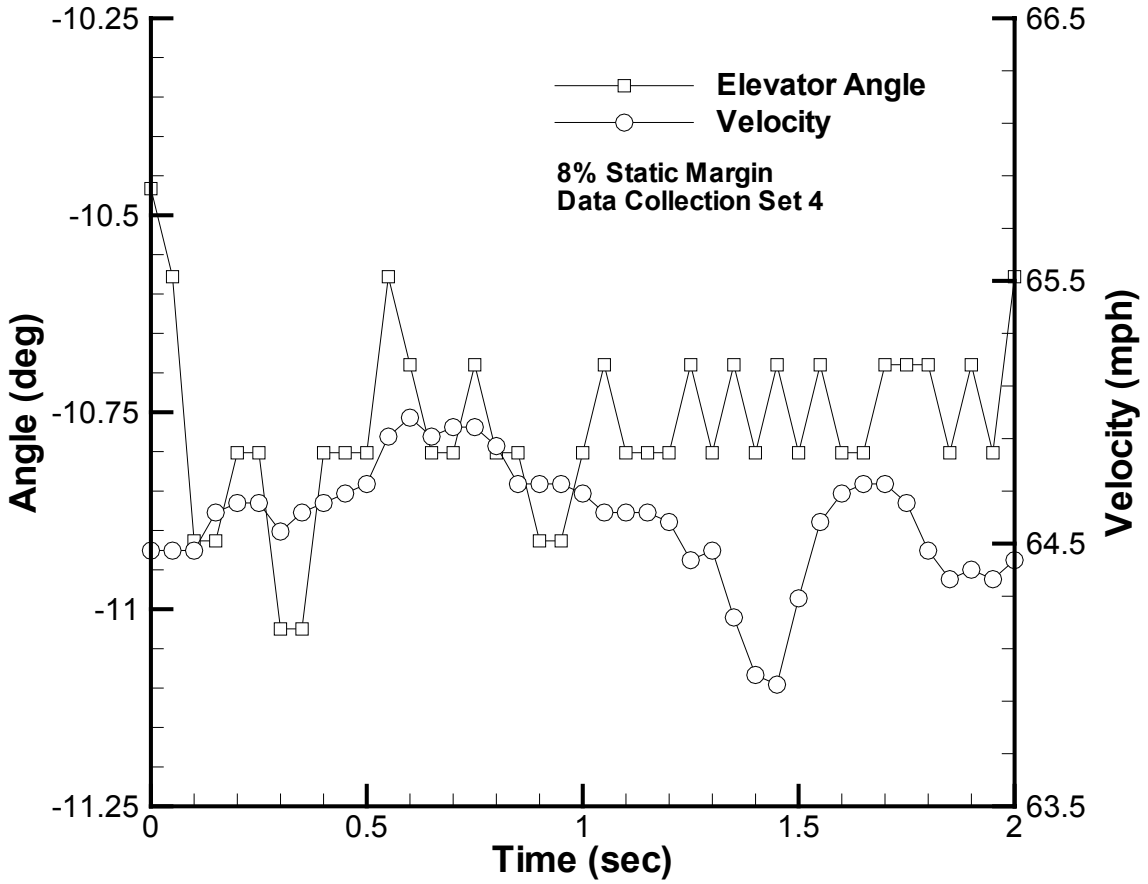

Figure 4.4: Steady State Data String

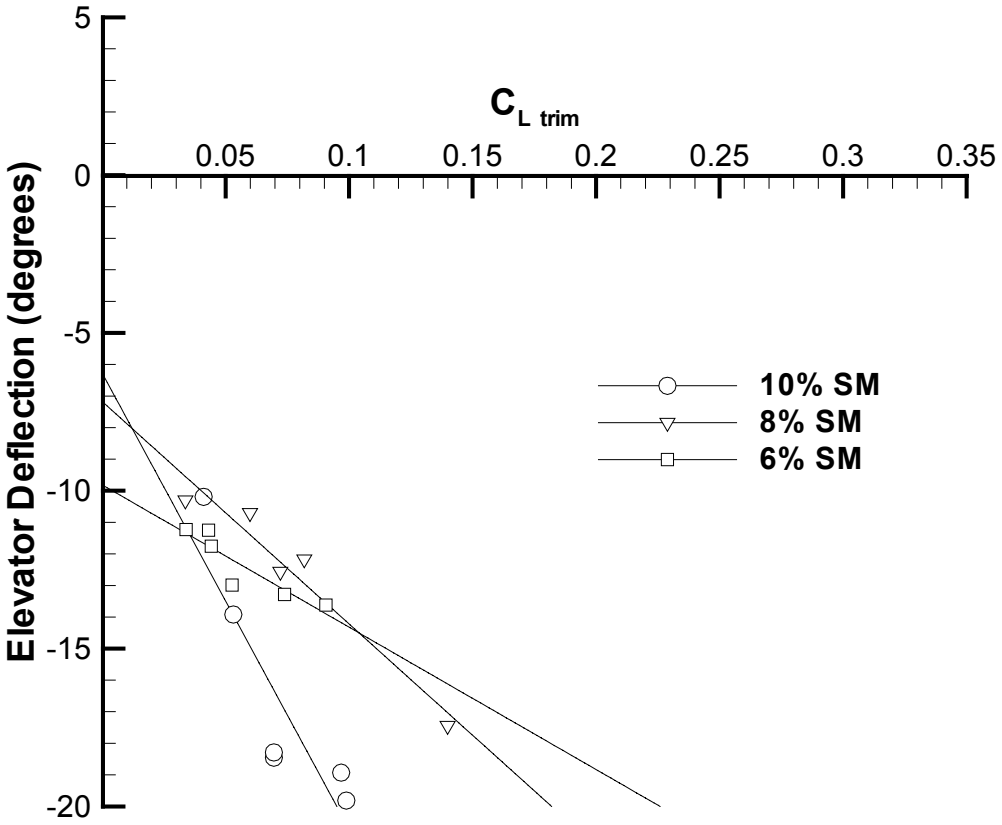

Figure 4.5: Steady State Results

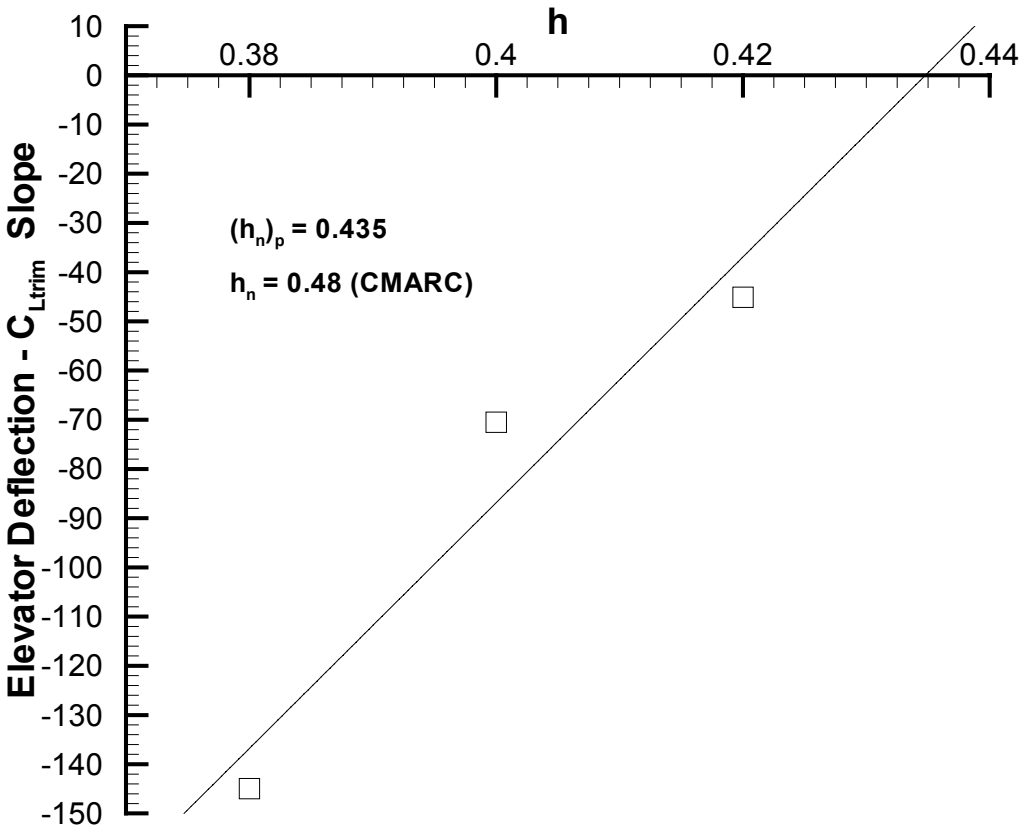

Figure 4.6: Steady State NP Results

APPENDIX -- Palindrome Flight Log

Flight Number	Run Time	Result
1	9:11	No Data Obtained
2	6:52	No Data Obtained
3	5:13	No Data Obtained
4	8:49	Data Obtained
5	7:05	Data Obtained
6	5:56	Data Obtained
7	2:07	Crash

Flight LOG - PALINDROME

Flight Conditions

Flight Number: 1
Test Locale: Perkins Field, Butner, NC.
Weather Conditions: Clear and sunny
Wind: Gusting to around 8
Date: 3/17/03
Time: 1700

Flight Plan:

1st of 3 tractor flights to obtain flight data at static margins of 6%, 8%, and 10%.
This flight: 6% SM.

Flight Events:

Estimated Time (min:sec)	Event	Pilot Comments
0:00	Engine Start	
3:00	Lift-off	
4:04	Comment	full throttle (coming out of turn)
5:13	Data Record Start	
5:17	Data Record Stop	
5:51	Data Record Start	
5:54	Data Record Stop	
6:21	Comment	half throttle
6:29	Data Record Start	
6:33	Data Record Stop	
7:10	Data Record Start	
7:13	Data Record Stop	
?	Data Record Start	
?	Data Record Stop	
8:58	Touch Down	
9:04	Complete Stop	
9:11	Engine off	

Notes:

Post flight: No data found.

Flight LOG - PALINDROME

Flight Conditions

Flight Number: 2
Test Locale: Perkins Field, Butner, NC.
Weather Conditions: Clear and sunny
Wind: Gusting to around 8
Date: 3/12/03
Time: 1728

Flight Plan:

2nd attempt for 1st of 3 tractor flights to obtain flight data at static margins of 6%, 8%, and 10%. This flight: 6% SM.

Flight Events:

Estimated Time (min:sec)	Event	Comments
0:00	Engine Start	
2:14	Lift-off	
3:05	Comment	Pilot: "3 clicks up"
3:21	Data Record Start	
3:23	Data Record Stop	
4:00	Data Record Start	
4:02	Data Record Stop	
4:27	Comment	Pilot: "Back on throttle"
4:42	Data Record Start	
4:44	Data Record Stop	
5:21	Data Record Start	
5:24	Data Record Stop	
5:51	Data Record Start	
5:53	Data Record Stop	
6:42	Touch Down	Hard bounce
6:50	Complete Stop	
6:52	Engine off	

Notes:

Post flight: No data found.

Flight LOG - PALINDROME

Flight Conditions

Flight Number: 3
Test Locale: Perkins Field, Butner, NC.
Weather Conditions: Clear and sunny
Wind: Gusting to around 8
Date: 3/12/03
Time: 1757

Flight Plan:

3rd attempt for 1st of 3 tractor flights to obtain flight data at static margins of 6%, 8%, and 10%. This flight: 6% SM.

Flight Events:

Estimated Time (min:sec)	Event	Comments
0:00	Engine Start	
2:09	Lift-off	
2:32	Data Record Start	
2:34	Data Record Stop	
3:11	Data Record Start	
3:12	Data Record Stop	
3:43	Data Record Start	
3:45	Data Record Stop	
4:00	Data Record Start	
4:01	Data Record Stop	
4:17	Data Record Start	
4:20	Data Record Stop	
4:40	Data Record Start	Hard bounce
4:42	Data Record Stop	
5:06	Touch Down	Sparks at wing tips
5:12	Complete Stop	
5:13	Engine off	

Notes:

Post flight: No data found.

Flight LOG - PALINDROME

Flight Conditions

Flight Number: 4
Test Locale: Perkins Field, Butner, NC.
Weather Conditions: Clear and sunny
Wind: Gusting to around 5 mph
Date: 3/20/03
Time: 1650

Flight Plan:

1st of 3 tractor flights to obtain flight data at static margins of 6%, 8%, and 10%. This flight: 6% SM.

Flight Events:

Estimated Time (min:sec)	Event	Comments
0:00	Engine Start	
2:51	Lift-off	
4:05	Data Record Start	
4:08	Data Record Stop	
5:24	Data Record Start	High Speed Pass
5:26	Data Record Stop	
5:58	Data Record Start	
6:00	Data Record Stop	
6:33	Data Record Start	
6:35	Data Record Stop	
7:09	Data Record Start	
7:11	Data Record Stop	
7:53	Data Record Start	
8:00	Data Record Stop	
8:43	Touch Down	
8:49	Complete Stop	
8:49	Engine off	

Notes:

High Elevator Rates. Mid Aileron Rates. Post flight pilot comment: aircraft did not respond well to elevator

Flight LOG - PALINDROME

Flight Conditions

Flight Number: 5
Test Locale: Perkins Field, Butner, NC.
Weather Conditions: Clear and sunny
Wind: Gusting to around 5 mph
Date: 3/20/03
Time: 1721

Flight Plan:

2nd of 3 tractor flights to obtain flight data at static margins of 6%, 8%, and 10%. This flight: 8% SM.

Flight Events:

Estimated Time (min:sec)	Event	Comments
0:00	Engine Start	
3:40	Lift-off	
4:13	Data Record Start	
4:15	Data Record Stop	
4:51	Data Record Start	High Speed Pass
4:53	Data Record Stop	
5:25	Data Record Start	
5:27	Data Record Stop	
5:45	Data Record Start	
5:46	Data Record Stop	
6:00	Comment	Pilot: "Taking it near stall"
6:02	Data Record Start	
6:06	Comment	Pilot: "Idle"
6:16	Comment	Pilot: "Throttling up"
6:18	Data Record Stop	
6:56	Touch-Down	
7:00	Engine off	
7:05	Complete Stop	

Notes:

Flight LOG - PALINDROME

Flight Conditions

Flight Number: 6
Test Locale: Perkins Field, Butner, NC.
Weather Conditions: Clear and sunny
Wind: Gusting to around 5mph
Date: 3/20/03
Time: 1746

Flight Plan:

3rd of 3 tractor flights to obtain flight data at static margins of 6%, 8%, and 10%. This flight: 10% SM.

Flight Events:

Estimated Time (min:sec)	Event	Comments
0:00	Engine Start	
2:12	Lift-off	
2:44	Data Record Start	
2:46	Data Record Stop	
3:05	Comment	Pilot: "High speed"
3:19	Data Record Start	
3:21	Data Record Stop	
3:38	Comment	Pilot: "Back on throttle"
3:52	Data Record Start	
3:54	Data Record Stop	
4:07	Data Record Start	Pilot: "Taking it near stall"
4:09	Data Record Stop	
4:25	Data Record Start	Pilot: "Idle"
4:30	Comment	Pilot: "Taking it near stall"
4:38	Data Record Stop	
4:38	Comment	Pilot: "Out (of stall) and throttling up"
5:05	Data Record Start	
5:06	Data Record Stop	
5:44	Touch-Down	
5:51	Complete Stop	
5:56	Engine Stop	

Notes:

Flight LOG - PALINDROME

Flight Conditions

Flight Number: 7
Test Locale: Perkins Field, Butner, NC.

Flight Plan:

1 flight attempt in pusher configuration 6% SM.

Flight Events:

Estimated Time (min:sec)	Event	Comments
0:00	Engine Start	
2:07	Crash	Palindrome flipped backwards off dolly

Notes:

Release mechanism failed simultaneously to winch release. Both booms snapped. Verticals split open. Engine mounts failed.